Dynamical functions of a 1D correlated quantum liquid

2008 J. Phys.: Condens. Matter 20 415103

(http://iopscience.iop.org/0953-8984/20/41/415103)

J. Phys.: Condens. Matter **20** (2008) 415103 (17pp) doi:10.1088/0953-8984/20/41/415103

Dynamical functions of a 1D correlated quantum liquid

J M P Carmelo[1], D Bozi[2] and K Penc[3]

[1] GCEP-Center of Physics, U. Minho, Campus Gualtar, P-4710-057 Braga, Portugal
[2] Centro de Física de Materiales, Centro Mixto CSIC-UPV/EHU, E-20018 San Sebastian, Spain
[3] Research Institute for Solid State Physics and Optics, H-1525 Budapest, POB 49, Hungary

E-mail: carmelo@fisica.uminho.pt

Received 9 January 2008, in final form 28 July 2008
Published 5 September 2008
Online at stacks.iop.org/JPhysCM/20/415103

Abstract

The dynamical correlation functions in one-dimensional electronic systems show power-law behaviour at low energies and momenta close to integer multiples of the charge and spin *Fermi momenta*. These systems are usually referred to as Tomonaga–Luttinger liquids. However, near well defined lines of the (k, ω) plane the power-law behaviour extends beyond the low-energy cases mentioned above, and also appears at higher energies, leading to singular features in the photoemission spectra and other dynamical correlation functions. The general spectral-function expressions derived in this paper were used in recent theoretical studies of the finite-energy singular features in photoemission of the organic compound tetrathiafulvalene–tetracyanoquinodimethane (TTF-TCNQ) metallic phase. They are based on a so-called pseudofermion dynamical theory (PDT), which allows us to systematically enumerate and describe the excitations in the Hubbard model starting from the Bethe ansatz, as well as to calculate the charge and spin object phase shifts appearing as exponents of the power laws. In particular, we concentrate on the spin-density $m \rightarrow 0$ limit and on effects in the vicinity of the singular border lines, as well as close to half filling. Our studies take into account spectral contributions from types of microscopic processes that do not occur for finite values of the spin density. In addition, the specific processes involved in the spectral features of TTF-TCNQ are studied. Our results are useful for the further understanding of the unusual spectral properties observed in low-dimensional organic metals and also provide expressions for the one- and two-atom spectral functions of a correlated quantum system of ultracold fermionic atoms in a 1D optical lattice with on-site two-atom repulsion.

(Some figures in this article are in colour only in the electronic version)

1. Introduction

The low-energy physics of correlated one-dimensional (1D) problems has some universal properties described by the Tomonaga–Luttinger liquid (TLL) [1]. In turn, a pseudofermion dynamical theory (PDT) beyond the TLL [2, 3] was recently used to study the finite-energy singular features in photoemission of the organic compound tetrathiafulvalene–tetracyanoquinodimethane (TTF-TCNQ) metallic phase [4]. While the PDT was originally introduced for the 1D Hubbard model, more recently other methods for the study of finite-energy spectral and dynamical functions of 1D correlated systems have been introduced [5, 6]. Both the finite-energy spectral-weight distributions studied by the PDT for the 1D Hubbard model and the methods of [5, 6] for other 1D correlated problems include power-law singularities near well defined branch lines with exponents depending on the interaction strength and the excitation momentum. In the limit of low energy the PDT correlation- and spectral-function expressions recover the usual low-energy TLL results [7].

Besides a renewed interest in the unusual spectral and dynamical properties of quasi-1D organic compounds [8, 9], recently there has been an increasing interest in those of interacting ultracold fermionic atoms in 1D optical lattices [10]. Quantum effects are strongest at low dimensionality, leading to unusual phenomena such as charge–spin

separation at all energies [8, 9]. Thus, the further understanding of the microscopic mechanisms behind the unusual spectral properties observed in low-dimensional correlated systems and materials is a topic of high scientific interest.

The 1D Hubbard model is one of the few realistic models for correlated electrons in a discrete lattice for which one can exactly calculate all the energy eigenstates and their energies [11–13]. It includes a first-neighbour transfer integral t, for electron hopping along the chain, and an effective on-site Coulomb repulsion U. For finite energy values the metallic phase of this model goes beyond the low-energy behaviour described by the usual TLL [1] and thus the study of spectral functions is a very involved many-electron problem. Fortunately, the construction of a pseudofermion description by means of a unitary transformation which slightly shifts the discrete momentum values of the corresponding pseudoparticles of [14, 15] leads to the PDT, whose energy spectrum has no residual-interaction energy terms. Therefore, such a description is suitable for the derivation of explicit expressions for these functions [2, 3, 7].

The PDT is a generalization for finite values of U of the scheme introduced in [16, 17] for large U values. It profits from the use of a description of the exact energy eigenstates in terms of occupancy configurations of several branches of pseudofermions. The ground state has finite occupancy of charge c and spin $s1$ pseudofermions only. Under the ground-state–excited-energy-eigenstate transitions, the pseudofermions and pseudofermion holes undergo elementary scattering events with the pseudofermions and pseudofermion holes created in these transitions. This leads to excited-state, interaction, density, and two-momenta-dependent two-pseudofermion phase shifts. The point is that the one- and two-electron spectral functions can be expressed in terms of pseudofermion determinants which are a functional of such phase shifts. Use of the PDT reveals that for finite values of U/t all singular one-electron spectral features of the model are of power-law type, controlled by negative exponents. Furthermore, the PDT line shapes associated with such exponents were found to correspond to the unusual charge and spin spectral features observed by photoemission experiments for the whole finite-energy band width in quasi-1D organic metals [18]. (The use of the dynamical density matrix renormalization group method [19] leads to results consistent with those obtained by the PDT.) Furthermore, when combined with the renormalization group, the use of the PDT reveals that a system of weakly coupled Hubbard chains is suitable for the successful description of the phase diagram observed in quasi-1D doped Mott–Hubbard insulators [20].

The low-energy physics of the model corresponds to the universal TLL behaviour and was studied by different techniques, such as conformal-field theory [21] and bosonization [22]. There are many investigations where the low-energy conformal invariance was combined with the model exact Bethe-ansatz solution in the study of the asymptotics of correlation functions and related quantities [1, 22]. As mentioned above, the studies of [7] confirm that in the limit of low energy the general finite-energy spectral- and correlation-function expressions provided by the PDT in [2] recover the correct behaviour given by conformal-field theory.

The main goal of this paper is to provide the details of an extension of the PDT introduced in [2, 3, 7] to initial ground states with spin density $m \rightarrow 0$, which was used in recent theoretical studies of the finite-energy singular features in photoemission of the TTF-TCNQ metallic phase [4]. The point is that such an extension involves spectral contributions that do not occur for finite values of the spin density and hence are not taken into account by the expressions of [2, 3, 7]. In order to introduce the generalized spectral-function expressions used in the recent studies of the TTF-TCNQ spectral features presented in short form in [4] we present here such an extension of the PDT.

The unusual spectral properties are mainly determined by the occupancy configurations in the excited states of the two-pseudofermion branches that have finite occupancies for the ground state. These are the charge $c0$ pseudofermion and spin $s1$ pseudofermion branches. The ground state corresponds to charge $c0$ pseudofermion (and spin $s1$ pseudofermion) finite occupancy for canonical-momentum values in the range $|\bar{q}| < q^0_{\mathrm{F}c0} = 2k_{\mathrm{F}}$ (and $|\bar{q}| < q^0_{\mathrm{F}s1} = k_{\mathrm{F}\downarrow}$) and charge $c0$ pseudofermion-hole (and spin $s1$ pseudofermion-hole) finite occupancy for canonical-momentum values in the range $2k_{\mathrm{F}} < |\bar{q}| < q^0_{c0} = \pi$ (and $k_{\mathrm{F}\downarrow} < |\bar{q}| < q^0_{s1} = k_{\mathrm{F}\uparrow}$). The values of the four deviations $\Delta\bar{q}_{\mathrm{F}c0,\pm1}$ and $\Delta\bar{q}_{\mathrm{F}s1,\pm1}$ in the two charge $\pm q^0_{\mathrm{F}c0} = \pm 2k_{\mathrm{F}}$ and two spin $\pm q^0_{\mathrm{F}s1} = \pm k_{\mathrm{F}\downarrow}$ *Fermi* points under each ground-state–excited-energy-eigenstate transition play a major role in the PDT.

We denote such deviations by $\Delta\bar{q}_{\mathrm{F}\alpha\nu,\iota}$, where $\alpha\nu = c0,\ s1$ and $\iota = \pm 1$. The spectral-weight distributions are controlled by the values of the following four associated parameters:

$$2\Delta^{\iota}_{\alpha\nu} = \left(\frac{\Delta\bar{q}_{\mathrm{F}\alpha\nu,\iota}}{[2\pi/L]}\right)^2; \qquad \alpha\nu = c0,\ s1; \quad \iota = \pm 1, \quad (1)$$

where $L \gg 1$ is the 1D lattice length within the use of periodic boundary conditions. According to the PDT, the contributions from ground-state transitions to subspaces spanned by sets of excited-energy eigenstates with the same values for the two charge parameters $2\Delta^{\pm1}_{c0}$ and two spin parameters $2\Delta^{\pm1}_{s1}$ fully determine the momentum k and energy ω dependence of the general finite-energy spectral functions in the small (k, ω)-plane region associated with the energy and momentum spectrum of these excited states [2, 3].

The general PDT finite-energy spectral-function expressions given in [2] refer to the metallic phase for initial ground states with spin densities m in the range $0 < m < n$, where n is the electronic density such that $0 < n < 1$. Actually, the expressions found in [2] refer to values of n such that the *Fermi*-point charge velocity v_{c0} is larger than the *Fermi*-point spin velocity v_{s1}. For finite values of U/t, this excludes densities n in the vicinity of half filling. One of our goals is to extend the studies of that reference to electronic densities such that $v_{s1} > v_{c0}$.

The general expressions of the exponents that control the singular features of the above finite-energy spectral-function expressions provide the correct zero spin-density values in

the limit $m \rightarrow 0$. Moreover, as given in equation (55) of [2], for excitations such that $2\Delta^{\iota}_{\alpha\nu} \neq 0$ for the two $\alpha\nu = c0$ charge and two $\alpha\nu = s1$ spin parameters the corresponding four-pseudofermion relative weights have the asymptotic expression provided in that equation. It follows that for zero spin excitations such that the four parameters $2\Delta^{\iota}_{\alpha\nu}$ where $\alpha\nu = c0, s1$ and $\iota = \pm 1$ are finite the general convolution function and corresponding pre-factor function $F_0(z)$ given in equations (61) and (62) of [2], respectively, provide the correct zero spin-density contributions to the spectral-function expressions in the limit of zero spin density. The point is that for densities in the ranges $0 < n < 1$ and $0 < m < n$ all ground-state–excited-energy-eigenstate transitions lead to finite values for these four parameters.

While some $m \rightarrow 0$ one- and two-electron excitations also lead to finite values for the two $\alpha\nu = c0$ charge and two $\alpha\nu = s1$ spin parameters $2\Delta^{\iota}_{\alpha\nu}$, there are also $m \rightarrow 0$ excitations for which one (or both) spin parameter(s) $2\Delta^{\pm 1}_{s1}$ vanishes (or vanish). In this case the corresponding $s1, \iota$ pseudofermion relative weights do not have the asymptotic expression provided in equation (55) of [2]. Nonetheless, we find in this paper that the contributions to the spectral-function expressions from ground-state transitions to the excited-energy eigenstates which span such excitations lead to convolution functions of the same general form as that provided in equation (61) of [2]. The only difference is that the pre-factor $F_0(z)$ of such convolution functions given in equation (62) of that reference is replaced by another suitable function derived in this paper and given in the appendix.

Since these convolution functions fully control all the different spectral-function contributions given in equations (66), (68), and (70) of [2], the derivation of all $m = 0$ contributions requires the use of such suitable pre-factors, which were taken into account in the studies of the TTF-TCNQ spectral features of [4] and we calculate in this paper. Interestingly, the different expressions found here for the pre-factor $F_0(z)$ are such that the corresponding pre-factors of the space and time asymptotic expressions of correlation functions [7] are continuous functions of m as $m \rightarrow 0$.

The extension of the expressions for the one- and two-electron spectral-weight distributions introduced in [2] for the 1D Hubbard model to the regime where $m \rightarrow 0$ involves taking into account contributions from transitions to subspaces spanned by excited states such that one, two, three, or even four out of the four parameters $2\Delta^{\iota}_{\alpha\nu}$, where $\alpha\nu = c0, s1$ and $\iota = \pm 1$, vanish. Note that according to equation (1) the value of the $\alpha\nu, \iota$ pseudofermion canonical-momentum Fermi points associated with $2\Delta^{\iota}_{\alpha\nu} = 0$ values remains unchanged under the corresponding ground-state–excited-state transitions. Such contributions do not exist for the $m > 0$ regime addressed in [2] but must be taken into account in the quantitative study of the spectral-weight distributions of the correlated metal at zero spin density. In this paper we also extend the one- and two-electron spectral-weight distributions of [2] to all electronic densities of the metallic phase. Although we do not consider the half-filling Mott–Hubbard insulator such that $v_{c0} = 0$, our expressions refer to all electronic densities of the metallic phase and thus also for those in the vicinity of unity.

Another problem solved in this paper is the derivation of explicit expressions for the spectral functions in the vicinity of the singular border lines, which again were used in the recent studies of the TTF-TCNQ spectral features of [4]. For that one-electron problem such border lines correspond to processes for which the extra charge and spin objects created upon removal or addition of the electron have exactly the same velocity. Such an equality of the charge and spin velocities occurs at well defined lines in the (k, ω) plane and leads to power-law singular behaviour along such border lines. In contrast to the power-law branch-line singular features studied in [2], which are controlled by momentum, U/t, and density dependent negative exponents, the border-line power-law singular features are controlled by a universal exponent given by $-1/2$, as given in equation (2) of [4]. Further details on the processes involved in the applications to TTF-TCNQ are also reported.

The paper is organized as follows. In section 2 we introduce the model and provide basic information about the pseudofermion description needed for our studies. In section 3 the general expressions required for the study of the finite-energy spectral-weight distributions of the metallic phase for initial $m \rightarrow 0$ ground states are calculated. This includes derivation of explicit expressions of the spectral functions in the vicinity of the singular border lines for density ranges $0 < n < 1$ and $0 \leqslant m < n$. In section 4 we use the expressions obtained in the previous section and in [2] to provide further details on the processes that contribute to the unusual photoemission spectrum of TTF-TCNQ. Finally, the concluding remarks are presented in section 5.

2. The problem and the pseudofermion description

Our study focuses on finite-ω $\mathcal{N}$-electron spectral-weight distributions of the following general form:

$$B^{l}_{\mathcal{N}}(k, \omega) = \sum_{f} |\langle f| \hat{O}^{l}_{\mathcal{N}}(k)|GS\rangle|^2 \times \delta(\omega - l[E_f - E_{\rm GS}]); \qquad l\omega > 0, \tag{2}$$

where $l = \pm 1$. We focus our attention on the cases of more physical interest which correspond to $\mathcal{N} = 1, 2$. In the above expression the general $\mathcal{N}$-electron operators $\hat{O}^{+1}_{\mathcal{N}}(k) \equiv \hat{O}^{\dagger}_{\mathcal{N}}(k)$ and $\hat{O}^{-1}_{\mathcal{N}}(k) \equiv \hat{O}_{\mathcal{N}}(k)$ carry momentum k, the f summation runs over the excited-energy eigenstates, the energy E_f corresponds to these states, and $E_{\rm GS}$ is the initial ground-state energy. The local operator $\hat{O}^{+1}_{\mathcal{N},j} \equiv \hat{O}^{\dagger}_{\mathcal{N},j}$ or $\hat{O}^{-1}_{\mathcal{N},j} \equiv \hat{O}_{\mathcal{N},j}$ is related to the corresponding momentum-representation operator $\hat{O}^{l}_{\mathcal{N}}(k)$ of equation (2) by a Fourier transform. As in [2], we use in expression (2) a momentum extended scheme such that $k \in (-\infty, +\infty)$.

We consider weight distributions (2) that refer to the Hubbard model in a 1D lattice with periodic boundary conditions and units such that the Planck constant and electronic lattice constant are unity,

$$\hat{H} = -t \sum_{j,\sigma} [c^{\dagger}_{j,\sigma} c_{j+1,\sigma} + \text{h.c.}] + U \sum_{j} \hat{n}_{j,\uparrow} \hat{n}_{j,\downarrow}. \tag{3}$$

Here $c^{\dagger}_{j,\sigma}$ ($c_{j,\sigma}$) creates (annihilates) one spin-projection $\sigma = \uparrow, \downarrow$ electron at site $j = 1, 2, \ldots, N_a$ and $\hat{n}_{j,\sigma} = c^{\dagger}_{j,\sigma} c_{j,\sigma}$. Let $N = N_{\uparrow} + N_{\downarrow}$ be the electronic number, N_a the number of lattice sites, and $n_{\sigma} = N_{\sigma}/L = N_{\sigma}/N_a$. N_a is assumed to be even and very large. The electronic densities $n = n_{\uparrow} + n_{\downarrow}$ and spin densities $m = n_{\uparrow} - n_{\downarrow}$ are in the ranges $0 < n < 1$ and $0 \leqslant m < n$, respectively. Except for corrections of order of $1/L$, the Fermi momenta are given by $k_{\rm F} = \pi n/2$ and $k_{{\rm F}\sigma} = \pi n_{\sigma}$.

The concept of a rotated electron plays a key role in the pseudofermion description. Concerning its relation to the holons, spinons, and $c0$ pseudoparticles whose occupancy configurations describe the energy eigenstates of the model (3), see [14]. Our studies do not involve directly the holons and spinons as defined in that reference. The charge $c\nu$ pseudofermions (and spin $s\nu$ pseudofermions) such that $\nu = 1, 2, 3, \ldots$ are 2ν-holon (and 2ν-spinon) composite quantum objects whose discrete momentum values are slightly shifted relative to those of the corresponding $c\nu$ pseudoparticles (and spin $s\nu$ pseudoparticles) studied in [14, 15]. Such momentum shifts cancel exactly the residual-interaction terms of the pseudoparticle energy spectrum. Otherwise, pseudoparticles and pseudofermions have the same properties.

According to the PDT of [2, 7], the charge $c0$ pseudofermions and spin $s1$ pseudofermions play the major role in the spectral properties. The holons (and spinons) which are not part of 2ν-holon composite $c\nu$ pseudofermions (and 2ν-spinon composite $s\nu$ pseudofermions) are the Yang holons (and HL spinons). These are invariant under the electron–rotated-electron unitary transformation and hence have a non-interacting character and do not contribute to the matrix elements between energy eigenstates of the spectral-weight distributions studied in this paper. We denote the numbers of $\alpha\nu$ pseudofermions and $\alpha\nu$ pseudofermion holes by $N_{\alpha\nu}$ and $N^{h}_{\alpha\nu}$, respectively, where $\alpha = c, s$ and $\nu = 0, 1, 2, \ldots$ for $\alpha = c$ and $\nu = 1, 2, \ldots$ for $\alpha = s$. (The value of $N^{h}_{\alpha\nu}$ is given in equations (B7) and (B8) of [14].)

As in [2], we use in this paper the notation $\alpha\nu \neq c0, s1$ branches, which refers to all $\alpha\nu$ branches except the $c0$ and $s1$ branches. Moreover, the summations (products) $\sum_{\alpha\nu}$, $\sum_{\alpha\nu=c0,\,s1}$, and $\sum_{\alpha\nu\neq c0,\,s1}$ ($\prod_{\alpha\nu}$, $\prod_{\alpha\nu=c0,\,s1}$, and $\prod_{\alpha\nu\neq c0,\,s1}$) run over all $\alpha\nu$ branches with finite $\alpha\nu$ pseudofermion occupancy in the corresponding state or subspace, the $c0$ and $s1$ branches only, and all $\alpha\nu$ branches with finite $\alpha\nu$ pseudofermion occupancy in the corresponding state or subspace except the $c0$ and $s1$ branches, respectively.

The pseudofermion description refers to a Hilbert subspace called the *pseudofermion subspace* (PS) in [2], in which the $\mathcal{N}$-electron excitations $\hat{O}^{l}_{\mathcal{N}}(k)|{\rm GS}\rangle$ are contained. The PS is spanned by the initial ground state and the excited-energy eigenstates originated from it by creation, annihilation, and particle–hole processes involving the generation of a finite number of active pseudofermion scattering centres, Yang holons, and HL spinons plus a vanishing or small density of low-energy and small-momentum $\alpha\nu = c0, s1$ pseudofermion particle–hole processes. It is convenient to classify these processes into three types, called processes (A), (B), and (C), as further discussed in the ensuing section.

The $\alpha\nu$-pseudofermion discrete canonical-momentum values have a functional character and read $\bar{q}_j = q_j + Q^{\Phi}_{\alpha\nu}(q_j)/L = [2\pi/L]I^{\alpha\nu}_j + Q^{\Phi}_{\alpha\nu}(q_j)/L$, where $j = 1, 2, \ldots, N^{*}_{\alpha\nu}$ and $N^{*}_{\alpha\nu} = N_{\alpha\nu} + N^{h}_{\alpha\nu}$. Here $Q^{\Phi}_{\alpha,\,\nu}(q_j)/2$ is an $\alpha\nu$ pseudofermion scattering phase shift given by

$$Q^{\Phi}_{\alpha\nu}(q_j)/2 = \sum_{\alpha'\nu'} \sum_{j'=1}^{N^{*}_{\alpha'\nu'}} \pi\, \Phi_{\alpha\nu,\,\alpha'\nu'}(q_j, q_{j'}) \times \Delta N_{\alpha'\nu'}(q_{j'}); \qquad j = 1, 2, \ldots, N^{*}_{\alpha\nu}, \tag{4}$$

where $\Delta N_{\alpha\nu}(q_j) = \Delta\mathcal{N}_{\alpha\nu}(\bar{q}_j)$ is the bare-momentum distribution function deviation $\Delta N_{\alpha\nu}(q_j) = N_{\alpha\nu}(q_j) - N^{0}_{\alpha\nu}(q_j)$ corresponding to the excited-energy eigenstate. This deviation is expressed in terms of the *bare momentum* $q_j = [2\pi I^{\alpha\nu}_j]/L$, which is carried by the $\alpha\nu$ pseudoparticles, where $I^{\alpha\nu}_j$ are the quantum numbers provided by the Bethe-ansatz solution [14].

Although the $\alpha\nu$ pseudoparticles carry bare momentum q_j, one can also label the corresponding $\alpha\nu$ pseudofermions by such a bare momentum. When we refer to the pseudofermion bare momentum q_j, we mean that q_j is the bare-momentum value that corresponds to the pseudofermion canonical momentum $\bar{q}_j = q_j + Q^{\Phi}_{\alpha\nu}(q_j)/L$. For the ground state the pseudofermion numbers are given by $N_{c0} = N$, $N_{s1} = N_{\downarrow}$, $N_{\alpha\nu} = 0$ for $\alpha\nu \neq c0, s1$. We call N^{0}_{c0} and N^{0}_{s1} the ground-state $c0$ and $s1$ pseudofermion numbers, respectively. As mentioned in the previous section, the ground-state $\alpha\nu = c0, s1$ bare-momentum distribution functions are such that there is pseudofermion occupancy for $|q| \leqslant q^{0}_{{\rm F}\alpha\nu}$ and unoccupancy for $q^{0}_{{\rm F}\alpha\nu} < |q| \leqslant q^{0}_{\alpha\nu}$, where in the thermodynamic limit the *Fermi-point* values are given by

$$q^{0}_{{\rm F}c0} = 2k_{\rm F}; \qquad q^{0}_{{\rm F}s1} = k_{{\rm F}\downarrow}. \tag{5}$$

Moreover, for that state the limiting bare-momentum values of both the $\alpha\nu = c0, s1$ and $\alpha\nu \neq c0, s1$ bands read

$$q^{0}_{c0} = \pi; \qquad q^{0}_{s1} = k_{{\rm F}\uparrow}; \qquad q^{0}_{c\nu} = [\pi - 2k_{\rm F}],\ \nu > 0; \qquad q^{0}_{s\nu} = [k_{{\rm F}\uparrow} - k_{{\rm F}\downarrow}], \qquad \nu > 1. \tag{6}$$

The ground-state $\alpha\nu = c0, s1$ densely packed bare-momentum distribution functions $N^{0}_{\alpha\nu}(q_j)$ are given in equations (C.1)–(C.3) of [14].

Under the ground-state–excited-energy-eigenstate transitions, the $\alpha\nu$ pseudofermions and $\alpha\nu$ pseudofermion holes undergo elementary scattering events with the $\alpha'\nu'$ pseudofermions and $\alpha'\nu'$ pseudofermion holes created in these transitions [2]. This leads to the elementary two-pseudofermion phase shifts $\pi\,\Phi_{\alpha\nu,\,\alpha'\nu'}(q_j, q_{j'})$ on the right-hand side of the overall scattering phase shift (4), as further discussed in [23]. Moreover, within the PDT the overall $\alpha\nu$ pseudofermion or hole phase shift,

$$Q_{\alpha\nu}(q_j)/2 = Q^{0}_{\alpha\nu}/2 + Q^{\Phi}_{\alpha\nu}(q_j)/2, \tag{7}$$

controls the spectral-weight distributions. Here $Q_{\alpha\nu}(q_j)/L$ gives the shift in the discrete canonical-momentum value $\bar{q}_j$ that arises due to the transition from the ground state to an excited-energy eigenstate and $Q^{0}_{\alpha\nu}/2$ can have the values

$Q^0_{\alpha\nu}/2 = 0, \pm\pi/2$ [2, 23]. In this paper we use boundary conditions such that $Q^0_{\alpha\nu}/2 = 0, -\mathrm{sgn}(k)\,\pi/2$, where k is the excited-state momentum relative to that of the initial ground state. Here we assume that for the latter state $N/2$ and N are odd and even numbers, respectively. $Q^0_{\alpha\nu}/L$ gives the shift in the discrete bare-momentum value q_j that arises as a result of the same transition.

The $\alpha\nu$ pseudofermion creation and annihilation operators $f^\dagger_{\bar{q}_j,\alpha\nu}$ and $f_{\bar{q}_j,\alpha\nu}$, respectively, have exotic anticommutation relations [2]. These anticommutators involve the overall phase shifts (7) and play a key role in the spectral properties. There are corresponding local operators $f^\dagger_{x_j,\alpha\nu}$ and $f_{x_j,\alpha\nu}$. Here x_j where $j = 1, 2, ..., N^*_{\alpha\nu}$ are the spatial coordinates of an $\alpha\nu$ effective lattice with $N^*_{\alpha\nu}$ sites. Each of the $N_{\alpha\nu}$ occupied sites of such a lattice corresponds to a well defined occupancy configuration of 2ν sites of the rotated-electron lattice. It turns out that the operators $f^\dagger_{x_j,\alpha\nu}$ and $f_{x_j,\alpha\nu}$ have simple anticommutation relations. Indeed, the exotic anticommutation relations of the operators and $f^\dagger_{\bar{q}_j,\alpha\nu}$ and $f_{\bar{q}_j,\alpha\nu}$ result from the form of the discrete canonical-momentum values $\bar{q}_j = q_j + Q^\Phi_{\alpha\nu}(q_j)/L = [2\pi/L]I^{\alpha\nu}_j + Q^\Phi_{\alpha\nu}(q_j)/L$.

There is a simple relation between the $f^\dagger_{x_j,c0}$ and $f_{x_j,c0}$ operators and those of the rotated electrons such that the former operators have anticommutation relations. To show that for branches $\alpha\nu \neq c0$ the operators $f^\dagger_{x_j,\alpha\nu}$ and $f_{x_j,\alpha\nu}$ also have anticommutation relations is a much more involved problem. The composite $\alpha\nu \neq c0$ pseudofermions emerge from corresponding $\alpha\nu \neq c0$ bond particles through a suitable Jordan–Wigner transformation [24]. The point is that such $\alpha\nu \neq c0$ bond particles live on the corresponding $\alpha\nu$ effective lattice and behave there as hard-core bosons. That interesting problem will be studied in detail elsewhere.

The charge and spin pseudofermion Fermi-point group velocities v_{c0} and v_{s1} also play an important role in our study. The velocity $v_{\alpha\nu}$ with $\alpha\nu = c0, s1$ is a particular case of the momentum dependent group velocity $v_{\alpha\nu}(q)$. Such velocities appear in all the spectral-weight distribution expressions of the metallic phase and are given by

$$v_{\alpha\nu}(q) = \frac{\partial\epsilon_{\alpha\nu}(q)}{\partial q}, \qquad \text{all branches;}$$
$$v_{\alpha\nu} \equiv v_{\alpha\nu}(q^0_{\mathrm{F}\alpha\nu}), \qquad \alpha\nu = c0, s1. \tag{8}$$

In the first expression $\epsilon_{\alpha\nu}(q)$ stands for the $\alpha\nu$ pseudofermion energy dispersion defined by equations (18)–(20) of [2]. In this paper and its appendix we often use a convention according to which the $\bar{\alpha}\bar{\nu} = c0, s1$ branch is that whose pseudofermion Fermi-point group velocity $v_{\bar{\alpha}\bar{\nu}}$ is such that

$$v_{\bar{\alpha}\bar{\nu}} = \min\{v_{c0}, v_{s1}\}. \tag{9}$$

3. Spectral-weight distributions for the metallic phase and $0 \leqslant m < n$

3.1. General spectral-function expressions

The pseudofermion elementary processes that generate the PS from the initial ground state belong to three types.

(a) Finite-energy and finite-momentum elementary $c0$ and $s1$ pseudofermion processes away from the corresponding Fermi points involving creation or annihilation of a finite number of pseudofermions plus creation of $\alpha\nu \neq c0, s1$ pseudofermions with bare-momentum values different from the limiting bare-momentum values $\pm q^0_{\alpha\nu}$.

(b) Zero-energy and finite-momentum processes that change the number of $c0$ and $s1$ pseudofermions at the $\iota = \mathrm{sgn}(q)\,1 = +1$ right and $\iota = \mathrm{sgn}(q)\,1 = -1$ left $c0$ and $s1$ Fermi points—these processes transform the ground-state densely packed bare-momentum occupancy configuration into an excited-state densely packed bare-momentum occupancy configuration. Furthermore, creation of a finite number of independent $-1/2$ holons and independent $-1/2$ spinons, including $-1/2$ Yang holons, $-1/2$ HL spinons, and $-1/2$ holons and $-1/2$ spinons associated with $c\nu$ pseudofermions of limiting bare momentum $q = \pm q^0_{c\nu} = \pm[\pi - 2k_{\mathrm{F}}]$ and $s\nu$ pseudofermions of limiting bare momentum $q = \pm q^0_{s\nu} = \pm[k_{\mathrm{F}\uparrow} - k_{\mathrm{F}\downarrow}]$, respectively.

(c) Low-energy and small-momentum elementary $c0$ and $s1$ pseudofermion particle–hole processes in the vicinity of the $\iota = \mathrm{sgn}(q)\,1 = +1$ right and $\iota = \mathrm{sgn}(q)\,1 = -1$ left $c0$ and $s1$ Fermi points, relative to the excited-state $\alpha\nu = c0, s1$ pseudofermion densely packed bare-momentum occupancy configurations generated by the above elementary processes (B).

Such processes generate excitations which can be classified by the values of a set of numbers and number deviations. For instance, $N^{\mathrm{phNF}}_{\alpha\nu}$ is the number of finite-momentum and finite-energy $\alpha\nu = c0, s1$ pseudofermion particle–hole processes of type (A). The quantum number $\iota = \mathrm{sgn}(q)1 = \pm 1$ refers to the right pseudofermion movers ($\iota = +1$) and left pseudofermion movers ($\iota = -1$) and $\Delta N^{\mathrm{F}}_{\alpha\nu,\,\iota}$ such that $\Delta N^{\mathrm{F}}_{\alpha\nu,\,\pm1}$ is the deviation in the number of $\alpha\nu$ pseudofermions at the right $(+1)$ and left (-1) Fermi points generated by the elementary processes (B). In turn, the deviation in the number of $\alpha\nu = c0, s1$ pseudofermions created or annihilated away from these points by elementary processes (A) is denoted by $\Delta N^{\mathrm{NF}}_{\alpha\nu}$.

The actual number of $\alpha\nu$ pseudofermions created or annihilated at the right $(+1)$ and left (-1) Fermi points by processes (B) is denoted by $\Delta N^{0,\mathrm{F}}_{\alpha\nu,\,\pm1}$. It is such that $\Delta N^{\mathrm{F}}_{\alpha\nu,\,\iota} = \Delta N^{0,\mathrm{F}}_{\alpha\nu,\,\iota} + \iota\, Q^0_{\alpha\nu}/2\pi$, where $Q^0_{\alpha\nu}/2$ is the scattering-less phase shift on the right-hand side of equation (7). Furthermore, $N^{\mathrm{F}}_{\alpha\nu,\,\iota}$ refers to the $\alpha\nu \neq c0, s1$ branches and is the number of $\alpha\nu$ pseudofermions of limiting bare momentum $q = \iota\, q^0_{\alpha\nu}$ such that $\iota = \pm1$ created by the elementary processes (B). The number of $\alpha\nu$ pseudofermions created away from the limiting bare-momentum values by processes (A) is called $N^{\mathrm{NF}}_{\alpha\nu}$.

A ground-state–excited-energy-eigenstate transition generated by elementary processes (A) and (B) leads to the energy and momentum spectrum $l\Delta E$ and $l\Delta P$ given in equations (28) and (29) of [2], respectively, where $l = +1$ or -1 depending on the specific spectral function (2) under consideration. Each such excited state is associated with a well defined point $(l\Delta E, l\Delta P)$ in the (k, ω)-plane. A key property

of the PDT is that the set or tower of excited states generated by elementary processes (C) from each excited-energy eigenstate generated by processes (A) and (B) have the same values for the two charge parameters $2\Delta_{c0}^{\pm 1}$ and two spin parameters $2\Delta_{s1}^{\pm 1}$ of equation (1) as the latter state. The transition to this tower of excited states generates the spectral weight in the vicinity of the corresponding point $(l\Delta E, l\Delta P)$. Thus, this weight is associated with the same value of the following functional, which plays a major role in the spectral properties:

$$\begin{aligned}\zeta_0 &= 2\Delta_{c0}^{+1} + 2\Delta_{c0}^{-1} + 2\Delta_{s1}^{+1} + 2\Delta_{s1}^{-1},\\ 2\Delta_{\alpha\nu}^{\iota} &= \left(\iota\,\Delta N_{\alpha\nu,\,\iota}^{\rm F} + \frac{Q_{\alpha\nu}^{\Phi}(\iota\, q_{{\rm F}\alpha\nu}^{0})}{2\pi}\right)^{2},\end{aligned} \tag{10}$$

where $\alpha\nu = c0,\ s1$ and $\iota = \pm 1$. Note that ζ_0 equals the sum of the four parameters of equation (1), which can be expressed in terms of the overall scattering phase shift of equation (4), as given in the second expression of equation (10). Such parameters are functionals of the pseudofermion occupancy configurations which describe the excited states generated by elementary processes (A) and (B).

The corresponding functional expressions are given in equations (12) and (40) of [2]. Thus, for each excited state generated from the initial ground state by processes (A) and (B) there is a subspace spanned by the set of excited states generated by processes (C) from the former excited state. Given the linear $\alpha\nu = c0,\ s1$ pseudofermion energy dispersion near the Fermi points, processes (C) lead to small momentum and energy values such that

$$\begin{aligned}k' &= \sum_{\alpha\nu=c0,\,s1}\sum_{\iota=\pm 1}\iota\,\frac{2\pi}{L}\,m_{\alpha\nu,\,\iota};\\ \omega' &= \sum_{\alpha\nu=c0,s1}\sum_{\iota=\pm 1}\frac{2\pi}{L}v_{\alpha\nu}m_{\alpha\nu,\iota}.\end{aligned} \tag{11}$$

Here $m_{\alpha\nu,\,\iota}$ is the number of elementary $\alpha\nu$ pseudofermion particle–hole processes of momentum $\iota[2\pi/L]$. Thus, elementary processes (C) generate a set of excited-energy eigenstates with energy $l\Delta E$ and momentum $l\Delta P$ given by those of the initial excited state generated from the ground state by processes (A) and (B), plus the small energy ω' and momentum k' provided in equation (11).

Within the PDT the general $\mathcal{N}$-electron spectral functions (2) factorize in terms of $\alpha\nu$ pseudofermion spectral functions. The probability amplitude $A_{\alpha\nu}^{(0,0)}$ appears in the expressions of the latter functions for $\alpha\nu = c0,\ s1$. It is associated with the canonical-momentum densely packed configurations generated by elementary processes (A) and (B) after the matrix elements between the ground state and the excited states generated by these processes are computed. Such a probability amplitude corresponds to the $\alpha\nu = c0,\ s1$ pseudofermion spectral-function lowest-peak weight given in equation (48) of [2]. It has the following approximate behaviour:

$$\begin{aligned}A_{\alpha\nu}^{(0,0)} &\approx \prod_{\iota=\pm 1} A_{\alpha\nu,\,\iota}^{(0,0)}\Big[1 + \mathcal{O}\Big(\frac{1}{N_a}\Big)\Big],\\ A_{\alpha\nu,\,\iota}^{(0,0)} &= \frac{f_{\alpha\nu,\,\iota}}{\left(N_a\, S_{\alpha\nu}^{0}\right)^{-1/2+2\Delta_{\alpha\nu}^{\iota}}}; \qquad \alpha\nu = c0,\ s1; \quad \iota = \pm 1.\end{aligned} \tag{12}$$

Here $2\Delta_{\alpha\nu}^{\iota}$ is the functional given in equation (1), and $f_{\alpha\nu,\,\iota}$ reads

$$\begin{aligned}f_{\alpha\nu,\,\iota} &= \sqrt{f\Big(Q_{\alpha\nu}(\iota q_{{\rm F}\alpha\nu}^{0}) + {\rm sgn}(k)\pi\Big)};\\ f_{\alpha\nu} &= \prod_{\iota=\pm 1} f_{\alpha\nu,\,\iota}; \qquad \alpha\nu = c0,\ s1.\end{aligned} \tag{13}$$

In this expression, k stands for the excited-state momentum relative to the initial ground state, $f(Q) = f(-Q)$ is the function defined in [17], which occurs on the right-hand side of equation (24) of that reference, and $f_{\alpha\nu}$ appears in spectral-function expressions introduced below. Moreover, $S_{\alpha\nu}^{0}$ is an n, m, and U/t dependent constant such that $S_{c0}^{0}\,S_{s1}^{0} \to 1$ both for $U/t \to 0$ and for $U/t \to \infty$ and $m \to 0$. (From [17] we learn that $S_{c0}^{0} \to \sin(\pi n)$ for $U/t \to \infty$ and $m \to 0$, and thus $S_{s1}^{0} \to 1/\sin(\pi n)$ in such a limit.) It is useful to introduce the following quantity:

$$D_0 = \prod_{\alpha\nu=c0,\,s1}\frac{S_{\alpha\nu}^{0}\,f_{\alpha\nu}}{(S_{\alpha\nu}^{0})^{[2\Delta_{\alpha\nu}^{+1}+2\Delta_{\alpha\nu}^{-1}]}}. \tag{14}$$

Another important piece of the $\alpha\nu = c0,\ s1$ pseudofermion spectral functions is the relative weight $a_{\alpha\nu,\,\iota}(m_{\alpha\nu,\,\iota})$ generated by the elementary processes (C) in the vicinity of the right ($\iota = +1$) and left ($\iota = -1$) Fermi points. When $2\Delta_{\alpha\nu}^{\iota} > 0$ the weight $a_{\alpha\nu,\,\iota}(m_{\alpha\nu,\,\iota})$ and its asymptotic expression are given in equations (52) and (55) of [2], respectively. The point is that when the excited states generated by processes (A) and (B) are such that $2\Delta_{\alpha\nu}^{\iota} = 0$ the relative weight $a_{\alpha\nu,\,\iota}(m_{\alpha\nu,\,\iota})$ reads instead

$$\begin{aligned}a_{\alpha\nu,\,\iota}(m_{\alpha\nu,\,\iota}) &= \delta_{m_{\alpha\nu,\,\iota},0};\\ 2\Delta_{\alpha\nu}^{\iota} &= 0; \qquad \alpha\nu = c0,\ s1; \quad \iota = \pm 1.\end{aligned} \tag{15}$$

Since for densities in the range $0 < n < 1$ and $0 < m < n$ the two charge parameters $2\Delta_{c0}^{\pm 1}$ and two spin parameters $2\Delta_{s1}^{\pm 1}$ are finite for all excited states, this case was not considered in the studies of [2].

As further discussed below, the general $\mathcal{N}$-electron spectral function given in equation (2) can be expressed in terms of the charge $c0$ and spin $s1$ spectral functions provided in equation (56) of [2]. Here we express the latter functions as follows:

$$\begin{aligned}&B_{Q_{\alpha\nu}}^{l,i}(k',\omega')\\ &= \frac{N_a}{2\pi}\int_{-\infty}^{+\infty}{\rm d}k''\int_{-\infty}^{+\infty}{\rm d}\omega''\,B_{Q_{\alpha\nu}}^{l,\iota,i}(k'-k'',\omega'-\omega'')\\ &\quad\times B_{Q_{\alpha\nu}}^{l,-\iota,i}\Big(k'',\omega''\Big); \qquad \alpha\nu = c0,s1; \quad \iota = \pm 1.\end{aligned} \tag{16}$$

The studies of [2] refer to the case where the two charge parameters $2\Delta_{c0}^{\pm 1}$ and two spin parameters $2\Delta_{s1}^{\pm 1}$ are finite. In that case the four relative weights $a_{\alpha\nu,\,\iota}(m_{\alpha\nu,\,\iota})$ such that $\alpha\nu = c0,s1$ and $\iota = \pm 1$ and their asymptotic expressions are of the form provided in equations (52) and (55) of [2], respectively, and thus the functions $B_{Q_{\alpha\nu}}^{l,\iota,i}(k',\omega')$ on the right-hand

side of equation (16) are given by [2]

$$B^{l,\iota,i}_{Q_{\alpha\nu}}(k',\omega') = \frac{A^{(0,0)}_{\alpha\nu,\iota}}{v_{\alpha\nu}}\, a_{\alpha\nu,\iota}\Big(\frac{l\,\omega'}{2\pi\, v_{\alpha\nu}/N_a}\Big)\,\delta\left(k'-\frac{\iota\,\omega'}{v_{\alpha\nu}}\right)$$
$$\approx \frac{f_{\alpha\nu,\iota}}{v_{\alpha\nu}\,\Gamma(2\Delta^{\iota}_{\alpha\nu})}\,\frac{\Theta(l\omega')}{\sqrt{N_a\,S^0_{\alpha\nu}}}\Big(\frac{l\omega'}{2\pi\,v_{\alpha\nu}\,S^0_{\alpha\nu}}\Big)^{2\Delta^{\iota}_{\alpha\nu}-1}$$
$$\times\,\delta\Big(k'-\frac{\iota\,\omega'}{v_{\alpha\nu}}\Big), \qquad (17)$$

where $\alpha\nu = c0,\, s1$ and $\iota = \pm 1$. The second expression corresponds to the asymptotic behaviour valid for small finite values of $l\omega'$.

However, when $2\Delta^{\iota}_{\alpha\nu} = 0$ the corresponding relative weight $a_{\alpha\nu,\iota}(m_{\alpha\nu,\iota})$ is of the form provided in equation (15) and thus the spectral function $B^{l,\iota,i}_{Q_{\alpha\nu}}(k',\omega')$ instead of being given by equation (17) reads

$$B^{l,\iota,i}_{Q_{\alpha\nu}}(k',\omega') = \frac{2\pi}{N_a}A^{(0,0)}_{\alpha\nu,\iota}\,\delta(k')\,\delta(\omega')$$
$$\approx 2\pi\, f_{\alpha\nu,\iota}\sqrt{\frac{S^0_{\alpha\nu}}{N_a}}\,\delta(k')\,\delta(\omega'); \qquad \alpha\nu = c0,\, s1;$$
$$\iota = \pm 1. \qquad (18)$$

In order to reach the correct spectral-function expressions for all electronic densities of the metallic phase and for $m \to 0$, several cases must be considered. The first corresponds to excited states such that the two charge parameters $2\Delta^{\pm 1}_{c0}$ and two spin parameters $2\Delta^{\pm 1}_{s1}$ are finite. The two functions on the right-hand side of equation (16) are of the form given in equation (17), and thus we find

$$B^{l,i}_{Q_{\alpha\nu}}(k',\omega') = \frac{L}{4\pi\, v_{\alpha\nu}}\,A^{(0,0)}_{\alpha\nu}\prod_{\iota=\pm 1}a_{\alpha\nu,\iota}\left(\frac{l[\omega'+\iota\, v_{\alpha\nu}\,k']}{4\pi\, v_{\alpha\nu}/N_a}\right)$$
$$\approx \frac{f_{\alpha\nu}}{4\pi\,v_{\alpha\nu}\,S^0_{\alpha\nu}}\prod_{\iota=\pm 1}\frac{\Theta(l[\omega'+\iota\,v_{\alpha\nu}\,k'])}{\Gamma(2\Delta^{\iota}_{\alpha\nu})}$$
$$\times\left(\frac{l[\omega'+\iota\,v_{\alpha\nu}\,k']}{4\pi\,v_{\alpha\nu}\,S^0_{\alpha\nu}}\right)^{2\Delta^{\iota}_{\alpha\nu}-1}, \qquad (19)$$

where $\alpha\nu = c0,\, s1$. The second expression corresponds to the asymptotic behaviour valid for small finite values of $l[\omega'+\iota\,v_{\alpha\nu}\,k']$. This function is that already given in equation (56) of [2]. (See the note[4] concerning a discrepancy of a factor of two between the function given here and that provided in equation (56) of [2] and how a misprint in the latter equation becomes an error, by propagating to other expressions of [2, 7].)

The second case occurs when the excited states are such that for the functions on the right-hand side of equation (16) one has that $2\Delta^{\iota}_{\alpha\nu} > 0$ and $2\Delta^{-\iota}_{\alpha\nu} = 0$. Then one must use in that equation the expression (17) for the function $B^{l,\iota,i}_{Q_{\alpha\nu}}(k',\omega')$ and that given in equation (18) for the function $B^{l,-\iota,i}_{Q_{\alpha\nu}}(k',\omega')$. This leads to the following expression for the function on the left-hand side of equation (16):

$$B^{l,i}_{Q_{\alpha\nu}}(k',\omega') = \frac{A^{(0,0)}_{\alpha\nu}}{v_{\alpha\nu}}\,a_{\alpha\nu,\iota}\Big(\frac{l\,\omega'}{2\pi\,v_{\alpha\nu}/N_a}\Big)\,\delta\Big(k'-\frac{\iota\,\omega'}{v_{\alpha\nu}}\Big)$$
$$\approx \frac{f_{\alpha\nu}}{v_{\alpha\nu}\,\Gamma(2\Delta^{\iota}_{\alpha\nu})}\,\Theta(l\omega')\Big(\frac{l\omega'}{2\pi\,v_{\alpha\nu}\,S^0_{\alpha\nu}}\Big)^{2\Delta^{\iota}_{\alpha\nu}-1}$$
$$\times\,\delta\Big(k'-\frac{\iota\,\omega'}{v_{\alpha\nu}}\Big), \qquad (20)$$

where $\alpha\nu = c0,\, s1$ and $\iota = \pm 1$.

Finally, the third case refers to excited states such that for the functions on the right-hand side of equation (16) one has that $2\Delta^{\iota}_{\alpha\nu} = 2\Delta^{-\iota}_{\alpha\nu} = 0$. In this case one must use in that equation the expression (18) for both the functions $B^{l,\iota,i}_{Q_{\alpha\nu}}(k',\omega')$ and $B^{l,-\iota,i}_{Q_{\alpha\nu}}(k',\omega')$. One then reaches the following expression for the function on the left-hand side of equation (16):

$$B^{l,i}_{Q_{\alpha\nu}}(k',\omega') = \frac{2\pi}{N_a}A^{(0,0)}_{\alpha\nu}\,\delta(k')\,\delta(\omega')$$
$$\approx 2\pi\, f_{\alpha\nu}\,S^0_{\alpha\nu}\,\delta(k')\,\delta(\omega'); \qquad \alpha\nu = c0,\, s1. \qquad (21)$$

The general PDT expression for the $\mathcal{N}$-electron spectral function given in equation (2) reads [2]

$$B^{l}_{\mathcal{N}}(k,\,\omega) = \sum_{i=0}^{\infty}c^{l}_{i}\sum_{\{\Delta N_{\alpha\nu}\},\,\{L_{\alpha,\,-1/2}\}}\left[\sum_{\{N^{\rm phNF}_{\alpha\nu}\},\,\{\Delta N^{\rm F}_{\alpha\nu,\iota}\},\,\{N^{\rm F}_{\alpha\nu,\iota}\}} B^{l,i}(k,\,\omega)\right], \qquad (22)$$

where $c^{l}_{0} = 1$, $l = \pm 1$, and for densities $0 < n < 1$ the summation over the numbers $N^{\rm phNF}_{\alpha\nu}$ is limited to finite values. On the right-hand side of equation (22), c^{l}_{i} is the constant of the operator expressions given in equations (32)–(34) of [3] such that $c^{l}_{i} \to 0$ as $U/t \to \infty$ for $i > 0$ and the function $B^{l,i}(k,\,\omega)$ is defined in equation (44) of [2]. The latter function is fully defined by the related function $\breve{B}^{l,i}(\Delta\omega,\,v)$. However, the second expression for $\breve{B}^{l,i}(\Delta\omega,\,v)$ given in equation (45) of [2] is only valid for $v_{c0} > v_{s1}$. For finite values of U/t this excludes electronic densities in the vicinity of unity.

Generalization of $\breve{B}^{l,i}(\Delta\omega,\,v)$ for the whole range of electronic densities of the metallic phase, including densities such that the spin and charge velocities obey the inequality $v_{s1} > v_{c0}$, leads to the following expression:

$$\breve{B}^{l,i}(\Delta\omega,\,v) = \frac{{\rm sgn}(v)}{2\pi}\int_0^{\Delta\omega}{\rm d}\omega'\int_{-{\rm sgn}(v)\Delta\omega/v_{\alpha\nu}}^{+{\rm sgn}(v)\Delta\omega/v_{\alpha\nu}}{\rm d}k'$$
$$\times\, B^{l,i}_{Q_{\bar{\alpha}\bar{\nu}}}\Big(\Delta\omega/v-k',\,\Delta\omega-\omega'\Big)\,B^{l,i}_{Q_{\alpha\nu}}\Big(k',\,\omega'\Big). \qquad (23)$$

In this equation, in those provided in the appendix, and in the whole of our analysis until section 3.2 we use a notation for the charge branch $c0$ and spin branch $s1$ such that $\alpha\nu = c0,\, s1$ when the branch index $\bar{\alpha}\,\bar{\nu}$ defined by equation (9) reads $\bar{\alpha}\,\bar{\nu} = s1,\, c0$, respectively. Moreover, in equation (23) $l = +1$ or -1 according to the $\mathcal{N}$-electron spectral function (2) under consideration, $\Delta\omega = (\omega - l\Delta E)$, $\Delta k = (k - l\Delta P)$, and $l\Delta E$ and $l\Delta P$ correspond to the general energy and momentum spectra given in equations (28) and (29) of [2], respectively,

[4] While the first expression provided in equation (56) of [2] is correct, there is a misprint in its second expression. It must be multiplied by two, which gives our expressions of equation (19). Such a misprint became an error that propagated to expression (62) of that reference, which must be multiplied by four. This gives our expression (A.1) of the appendix for $v_{c0} > v_{s1}$. Furthermore, it propagated to the first paper of [7] so that the pre-factor given in equation (50) of the latter paper must also be multiplied by four. Finally, while the exponent of expression (73) of [2] is correct, the pre-factor is a poor approximation.

which is generated by elementary processes (A) and (B), $i = 0, 1, 2, \ldots$, and for $i > 0$ the index $i = 1, 2, \ldots$ is a positive integer number which increases for increasing values of the number of extra pairs of creation and annihilation rotated-electron operators in the expressions of the pseudofermion operators associated with the function $\breve{B}^{l,i}(\Delta\omega, v)$ relative to that of the pseudofermion operators of the $i = 0$ function $\breve{B}^{l,0}(\Delta\omega, v)$ [2]. Expression (23) is valid for the whole (k, ω)-plane, except for k and ω values such that $\omega \approx \iota\, v_{\alpha\nu}(k - lk_0) + l\omega_0$, where $\alpha\nu = c0, s1, \iota = \pm 1, \omega_0$ and k_0 are provided in equations (32) and (34) of [2].

The velocity v appearing in the argument of the function (23) plays an important role in our study and is given by

$$v = \frac{\Delta\omega}{\Delta k} = \frac{(\omega - l\Delta E)}{(k - l\Delta P)}; \qquad \mathrm{sgn}(v)\, 1 = \mathrm{sgn}(\Delta k)\, l; \quad |v| > v_{\bar{\alpha}\bar{\nu}}. \tag{24}$$

The inequality $|v| > v_{\bar{\alpha}\bar{\nu}}$ follows from the structure of the spectrum of equation (31) of [2].

When at least one of the two parameters $2\Delta^{\pm 1}_{\alpha\nu}$ and two parameters $2\Delta^{\pm 1}_{\bar{\alpha}\bar{\nu}}$ is finite, use of the general expression (23) for the function $\breve{B}^{l,i}(\Delta\omega, v)$ for small finite values of $l\Delta\omega = l(\omega - l\Delta E)$ with $B^{l,i}_{Q_{\alpha\nu}}(k', \omega')$ and $B^{l,i}_{Q_{\bar{\alpha}\bar{\nu}}}(k', \omega')$ equalling the suitable expressions provided in equations (19)–(21) leads to the following asymptotic behaviour for that convolution function:

$$\breve{B}^{l,i}(\Delta\omega, v) \approx \frac{F_0(1/v)}{4\pi\sqrt{v_{c0}\, v_{s1}}}\, \Theta\Big(l\Delta\omega\Big)\Big(\frac{l\Delta\omega}{4\pi\sqrt{v_{c0}\, v_{s1}}}\Big)^{-2+\zeta_0}. \tag{25}$$

Here $i = 0, 1, 2, \ldots$, $l = \pm 1$, ζ_0 is the functional provided in equation (10), and the pre-factor function $F_0(z)$ is given in the appendix. In turn, if all the above four parameters vanish, we find by use of expression (23) with $B^{l,i}_{Q_{\alpha\nu}}(k', \omega')$ and $B^{l,i}_{Q_{\bar{\alpha}\bar{\nu}}}(k', \omega')$ of the form given in equation (21) that

$$\breve{B}^{l,i}(\Delta\omega, v) = \bar{B}^{l,i}(\Delta\omega, \Delta k) = 2\pi\, D_0\, \delta(\Delta\omega)\delta(\Delta k), \tag{26}$$

where D_0 is defined in equation (14), in agreement with the first expression of equation (59) of [2] for $\zeta_0 = 0$.

Depending on the values of the two parameters $2\Delta^{\pm 1}_{\alpha\nu}$ and two parameters $2\Delta^{\pm 1}_{\bar{\alpha}\bar{\nu}}$, we consider in the appendix seven cases where by use of equations (19)–(21), (23), and (25) a set of alternative expressions for the pre-factor function $F_0(z)$ on the right-hand side of the latter equation can be derived and is given in the appendix. Expressions (A.1)–(A.7) of the appendix provide a generalization of the pre-factor function $F_0(z)$ given in equation (62) of [2]. The latter function corresponds to the general function (A.1) of the appendix for $\alpha\nu = c0$ (see footnote 4). The recent studies of [4] on the finite-energy spectral features of the organic compound TTF-TCNQ use the functions (A.1)–(A.7) of the appendix derived in this paper.

Importantly, general spectral-function expressions for all electronic densities of the metallic phase are obtained by replacing the spin velocity v_{s1} by $v_{\bar{\alpha}\bar{\nu}}$ in the limits of the variable z integrations of expressions (66) and (B.14) of [2] and both in the limits of the variable z integrations and arguments of the theta-functions of expressions (71), (B.17), and (B.18) of the same reference. After such replacements, equations (66), (68), (70), and (71) of [2] with the pre-factor function $F_0(z)$ given in equations (A.1)–(A.7) of the appendix provide general spectral-function expressions for all electronic densities of the metallic phase and spin densities in the range $0 \leqslant m < n$. However, note that, while the branch index $\bar{\alpha}\bar{\nu}$ is that defined by equation (9), the branch indices $\alpha\nu$ and $\alpha'\nu'$ of equations (66) and (B.14) of [2] correspond to the two created quantum objects and in contrast to the branch index $\alpha\nu$ of equations (23)–(26) and (A.1)–(A.7) of the appendix there are no restrictions imposing that such branch indices are different or equal to the branch index $\bar{\alpha}\bar{\nu}$, the same applying to the branch index $\alpha\nu$ of equations (70), (71), (B.17), and (B.18) of that reference.

It is straightforward to show that the double Fourier transform of the function (18) equals that of the function (17) as $2\Delta^{\iota}_{\alpha\nu} \to 0$. It follows that the asymptotic expression of the correlation function given in equation (32) of [7] is of the general form provided in equation (52) of that reference independently of whether all four parameters $2\Delta^{\iota}_{\alpha\nu}$ where $\alpha\nu = c0, s1$ and $\iota = \pm 1$ are finite, or some of these parameters vanish. Thus, the different expressions (A.1)–(A.7) of the appendix for the pre-factor $F_0(z)$ of the convolution function (25) are not associated with different pre-factors for the corresponding correlation-function expression (52) of [7]. The pre-factor of the latter function is always of the form given in equation (50) of that reference (see footnote 4).

3.2. Explicit spectral-function expressions in the vicinity of the border lines

The singular features of the $\mathcal{N}$-electron spectral functions (2) are of power-law type. The power-law branch-line singular features of general form given in equations (68) and (71) of [2] are controlled by non-classic interaction, density, and momentum dependent exponents. The spectral feature of general form given in equations (66) of that reference can also include power-law singular features called border lines. However, the studies of [2] did not provide an explicit general expression for the k and ω dependence in the vicinity of the border lines. Here we provide such an expression and find that for the border lines the power-law exponent has an universal value given by $-1/2$.

The shape $\omega = \omega_{\mathrm{BL}}(k)$ of a border line is defined by the following parametric equations [2]:

$$\omega_{\mathrm{BL}}(k) = l[\,\omega_0 + c'_1\,\epsilon_{\alpha'\nu'}(q') + c''_1\,\epsilon_{\alpha''\nu''}(q'')] \times \delta_{v_{\alpha'\nu'}(q'),\, v_{\alpha''\nu''}(q'')}, \qquad k = lk_{\alpha'\nu',\,\alpha''\nu''}(q',\, q'')\,\delta_{v_{\alpha'\nu'}(q'),\, v_{\alpha''\nu''}(q'')}. \tag{27}$$

Here q' and q'' are the bare-momentum values of the $\alpha'\nu'$ and $\alpha''\nu''$, respectively, pseudofermion or pseudofermion-hole scattering centres created by processes (A), $c'_1, c''_1 = +1$ for pseudofermion creation and $c'_1, c''_1 = -1$ for pseudofermion-hole creation, ω_0 is the finite-energy parameter given in equation (32) of [2], and $k_{\alpha'\nu',\,\alpha''\nu''}(q',\, q'')$ is the momentum spectrum provided in equations (64) and (65) of that reference. As for equations (66) and (B.14) of [2] and in contrast to

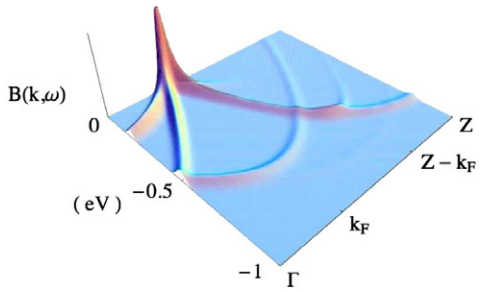

Figure 1. Full theoretical line shape of the one-electron removal spectral-weight distribution found in [4] to fit the corresponding spectral features of TTF-TCNQ. The spectrum shown here is rotated relative to that shown in figure 2 of that reference. It includes both the TTF related spectral features for $n = 1.41$; $t = 0.35$ eV; $U/t = 5.61$ and those of TCNQ for $n = 0.59$; $t = 0.40$ eV; $U/t = 4.90$, respectively.

the branch index $\alpha\nu$ of equations (23)–(26) and (A.1)–(A.7) of the appendix, there are no restrictions imposing that the branch indices $\alpha'\nu'$ and $\alpha''\nu''$ of the two created scattering centres are different or equal to the branch index $\bar{\alpha}\bar{\nu}$ defined by equation (9).

By use of methods similar to those used in [2] for other weight distributions, we find that the spectral function has the following singular behaviour in the vicinity and just below ($l = +1$) or above ($l = -1$) the border line:

$$B^{l}_{\mathcal{N}}(k,\,\omega) \approx \frac{2\,\Theta\Big(\Omega - l[\omega_{\rm BL}(k) - \omega]\Big)}{\pi\,C_c\,C_s\,\zeta_0(q',\,q'')\,\sqrt{|a_{\alpha'\nu'}(q')| + |a_{\alpha''\nu''}(q'')|}} \times \left[\int_{-1/v_{\bar{\alpha}\bar{\nu}}}^{+1/v_{\bar{\alpha}\bar{\nu}}} {\rm d}z\; F_0(z)\right] \times \left(\frac{\Omega}{4\pi\sqrt{v_{c0}\,v_{s1}}}\right)^{\zeta_0(q',\,q'')} \left(\frac{2l[\omega_{\rm BL}(k) - \omega]}{v_{c0}\,v_{s1}}\right)^{-\frac{1}{2}}, \qquad (28)$$

where $a_{\alpha\nu}(q) = \partial v_{\alpha\nu}(q)/\partial q$. In turn, just above ($l = +1$) or below ($l = -1$) the line the weight distribution reads

$$B^{l}_{\mathcal{N}}(k,\,\omega) \approx \frac{2\,\Theta\Big(\Omega - l[\omega - \omega_{\rm BL}(k)]\Big)}{\pi\,C_c\,C_s\,\zeta_0(q',\,q'')\,\sqrt{|a_{\alpha'\nu'}(q')| + |a_{\alpha''\nu''}(q'')|}} \times \left\{\Theta\left(v_{\bar{\alpha}\bar{\nu}}\left[1 - \frac{l[\omega - \omega_{\rm BL}(k)]}{\Omega}\right] - |v_{\alpha'\nu'}(q')|\right) \times \int_{\frac{-1}{v_{\bar{\alpha}\bar{\nu}}}}^{\frac{1}{v_{\bar{\alpha}\bar{\nu}}}} {\rm d}z\; F_0(z) + {\rm sgn}(q') \times \theta\left(|v_{\alpha'\nu'}(q')| - v_{\bar{\alpha}\bar{\nu}}\left[1 - \frac{l[\omega - \omega_{\rm BL}(k)]}{\Omega}\right]\right) \times \int_{-\frac{{\rm sgn}(q')\,1}{v_{\bar{\alpha}\bar{\nu}}}}^{\frac{1}{v_{\alpha'\nu'}(q')}\left(1 - \frac{l[\omega - \omega_{\rm BL}(k)]}{\Omega}\right)} {\rm d}z\; F_0(z)\right\} \times \left[\left(\frac{\Omega}{4\pi\sqrt{v_{c0}\,v_{s1}}}\right)^{\zeta_0(q',\,q'')} - \left(\frac{l[\omega - \omega_{\rm BL}(k)]}{4\pi\sqrt{v_{c0}\,v_{s1}}\,[1 - z\,v_{\alpha'\nu'}(q')]}\right)^{\zeta_0(q',\,q'')}\right] \times \left(\frac{2l[\omega - \omega_{\rm BL}(k)]}{v_{c0}\,v_{s1}}\right)^{-\frac{1}{2}}, \qquad (29)$$

where $\theta(x) = 0$ for $x \leqslant 0$ and $\theta(x) = 1$ for $x > 0$, Ω is the energy cutoff of elementary processes (C) defined in [2], $\zeta_0 = \zeta_0(q',\,q'')$ is the functional given in equation (10) for the excited states which contribute to the weight distribution (66) of that reference, and C_c and C_s are defined in equation (68) of [3].

4. Applications of the pseudofermion dynamical theory to the spectrum of TTF-TCNQ

As discussed in [4], the spectral-weight distribution of TTF-TCNQ is fully determined by the occupancy configurations of the c and $s1$ pseudofermions in the one-electron excited states. The studies of that reference reveal that for electronic density $n = 1.41$ the electron removal spectrum calculated for $t = 0.35$ eV and $U = 1.96$ eV ($U/t = 5.61$) yields the best agreement with the TTF related experimental dispersions. In turn, for electronic density $n = 0.59$ an almost perfect agreement with the TCNQ related experimental dispersions is reached for the finite-energy-electron-removal spectrum calculated for $t = 0.40$ eV and $U = 1.96$ eV ($U/t = 4.90$) [4, 18].

If one profits from the model particle–hole symmetry, one can achieve the one-electron removal spectrum at $n = 1.41$ and a given U/t value from the one-electron addition spectrum at $n = 0.59$ and the same value of U/t. The full theoretical line shape of the one-electron removal spectral-weight distribution found in [4] to fit the corresponding spectral features of TTF-TCNQ is shown in figure 1. Note that here such a spectrum is rotated relative to that shown in figure 2 of that reference.

Let us consider the processes that contribute to the spectrum of figure 1. Each of the corresponding spectral-weight contributions to the full one-electron spectrum plotted

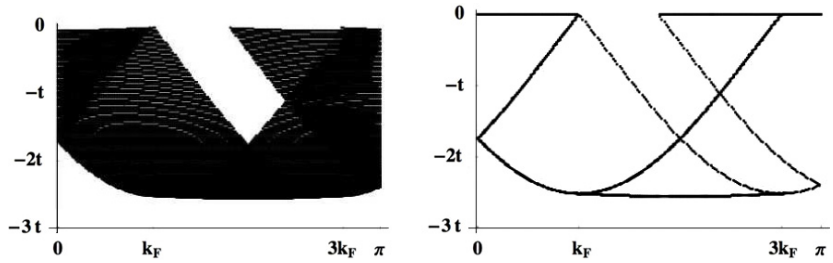

Figure 2. The region of the (k, ω) plane with a finite one-electron removal spectral weight obtained by running over all the momentum values of the $c0$ and $s1$ momentum distribution deviations of equations (32) and (33) for $U/t = 100$, $n = 0.59$, and $m \to 0$. The corresponding branch and border lines are also plotted.

in this figure are obtained by use of the PDT expressions provided in the previous section and [2]. In addition to the values of U/t and n specific to TTF-TCNQ, some of the spectral contributions plotted below refer to variations in these parameters. This allows us to study how the spectral features evolve under such variations. The study of the spectral-weight pieces contributing to the full spectrum plotted in figure 1 allows the identification of the contributions from the different expressions considered in the previous section and [2], including the border-line expressions derived in this paper and provided in equations (28) and (29).

The one-electron removal spectral-weight distribution of figure 1 has two main contributions, referring to the TCNQ and TTF related spectral features, respectively. The TCNQ related spectrum is obtained by considering the one-electron removal spectral function for $n = 0.59$; $t = 0.40$ eV; $U/t = 4.90$. In turn, we profit from the model particle–hole symmetry to derive the TTF related photoemission spectrum for $n = 1.41$; $t = 0.35$ eV; $U/t = 5.61$ from the corresponding one-electron addition spectrum for $n = 0.59$; $t = 0.35$ eV; $U/t = 5.61$ and changing the energy and momentum signs.

Nearly the whole one-electron removal spectral weight corresponds to excitations described by the following deviations from the ground-state $N_{\alpha\nu}$ $\alpha\nu$ pseudofermion numbers and $N^h_{\alpha\nu}$ $\alpha\nu$ pseudofermion-hole numbers where $\alpha\nu = c0, s1$:

$$\Delta N_{c0} = -\Delta N^h_{c0} = -1; \qquad \Delta N_{s1} = -\Delta N^h_{s1} = -1, \tag{30}$$

and with the numbers $Q^0_{\alpha\nu}/2$ appearing on the right-hand side of equation (7) reading

$$Q^0_{c0}/2 = \pm\pi/2; \qquad Q^0_{s1}/2 = 0. \tag{31}$$

If we consider bare-momentum continuum values, the general deviations read

$$\Delta N_{c0}(q) = -\frac{2\pi}{L}\,\delta(q - q_1) - \frac{\pi}{L}\,\delta(q \mp 2k_{\rm F}) + \frac{\pi}{L}\,\delta(q \pm 2k_{\rm F}); \qquad q_1 \in [-2k_{\rm F},\ +2k_{\rm F}] \tag{32}$$

$$\Delta N_{s1}(q) = -\frac{2\pi}{L}\,\delta(q - q'_1); \qquad q'_1 \in [-k_{\rm F\downarrow},\ +k_{\rm F\downarrow}],$$

and thus

$$\Delta N_{s1}(q) = -\frac{2\pi}{L}\,\delta(q - q'_1); \qquad q'_1 \in [-k_{\rm F},\ +k_{\rm F}] \tag{33}$$

as $m \to 0$ for the initial ground state. Such deviations and numbers (31) are then used in the general functional $Q_{\alpha\nu}(q_j)/2$ given in equation (7), whose functional $Q^{\Phi}_{\alpha\nu}(q_j)/2$ is defined in equation (4). Such a procedure leads to

$$Q_{c0}(q)/2 = \pm\pi/2 - \pi\,\Phi_{c0,\,c0}(q, q_1) - \pi\,\Phi_{c0,\,c0}(q, \mp 2k_{\rm F})/2 + \pi\,\Phi_{c0,\,c0}(q, \pm 2k_{\rm F})/2 - \pi\,\Phi_{c0,\,s1}(q, q'_1), \tag{34}$$

and

$$Q_{s1}(q)/2 = -\pi\,\Phi_{s1,\,c0}(q, q_1) - \pi\,\Phi_{s1,\,c0}(q, \mp 2k_{\rm F})/2 + \pi\,\Phi_{s1,\,c0}(q, \pm 2k_{\rm F})/2 - \pi\,\Phi_{s1,\,s1}(q, q'_1), \tag{35}$$

respectively.

The creation of the holes in the $c0$ and $s1$ bands whose energy dispersions are plotted in figures 6 and 7 of [15], respectively, corresponds for $U/t = 100$, $n = 0.59$, and $m \to 0$ to a finite spectral-weight distribution in the region of the (k, ω) plane shown in figure 2. The lines associated with the branch lines and border lines in the finite-weight distribution are also shown. Most lines of the one-electron spectral-weight distribution plotted in figure 1 corresponding to power-law singularities are of the branch-line type. In contrast to the border-line singularities of expressions (28) and (29), whose exponent $-1/2$ is momentum and U/t independent, that controlling the branch-line power-law singularities is both momentum and interaction dependent. Near a branch line the general expression of the weight distribution is that provided in equation (70) of [2]. Only for momentum and interaction values where the exponent of that expression is negative is the corresponding line called a branch line. For the limit $m \to 0$ considered here the pre-factor function $F_0(z)$ appearing in such a branch-line expression is that given in equations (A.1)–(A.7) of the appendix. The expressions provided in the latter equations are a generalization of the pre-factor function $F_0(z)$ of equation (62) of [2]. The latter applies solely when $0 < n < 1$ and $0 < m < n$.

In figure 3 the same finite one-electron removal spectral-weight region and corresponding lines are shown for the $U/t = 4.9$, $n = 0.59$, and $m \to 0$ values suitable for the TCNQ related spectral features. Consistent with the U/t dependence of the energy bandwidth of the $s1$ pseudofermion dispersion plotted in figure 7 of [15], note that the border line connecting the minimum energy points of the two $c0$-branch lines has $v_{c0}(q) = v_{s1}(q') \approx 0$. Upon decreasing the U/t value to that $U/t = 4.9$ suitable for the TCNQ related spectral features of figure 1, such a border line acquires a curvature. The curvature achieved at $U/t = 4.9$ is that behind the agreement found in [4] between the PDT predictions and the photoemission spectral features of TTF-TCNQ. This agreement is not obtained for larger or smaller values of U/t.

The (negative exponent) $c0$ branch line of the weight distributions of figures 2 and 3 runs between the excitation momenta $-k_{\rm F}$ and $3k_{\rm F}$ and the $s1$ branch line from $-k_{\rm F}$ to $k_{\rm F}$. The corresponding power-law momentum dependent exponents are plotted in figure 4 for $n = 0.59$, $m \to 0$, and several values of U/t. The $c0$ branch-line segment between $-k_{\rm F}$ and 0 is folded in the positive momentum region. While the negative $c0$ branch-line exponent is smaller for large U/t, the negative $s1$ branch-line exponent is smaller for smaller values of U/t. In order to illustrate how systematic variations in the parameters lead to the evolution of the spectral features, the same exponents as in figure 4 are plotted in figure 5 as a function of momentum for $U/t = 10$, $m \to 0$, and several values of n.

The use in the general PDT expressions provided in this paper and in [2] of the specific $c0$ and $s1$ momentum deviations of equations (32) and (33) and corresponding functionals given in equations (34) and (35) leads for $U/t = 100$, $n = 0.59$, and $m \to 0$ to the one-electron removal spectral-weight distribution plotted in figure 6. Such a large-U/t distribution is quite similar to the function $B(k, \omega)$ plotted in figure 1 of [16]

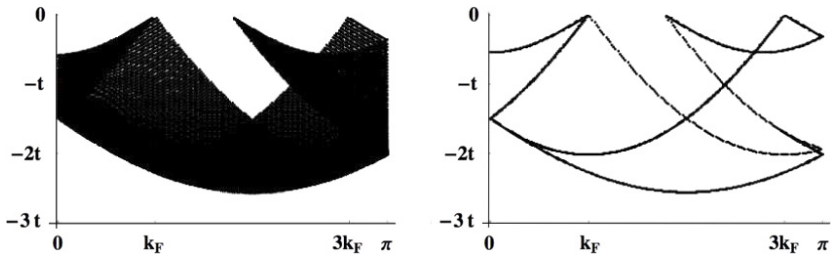

Figure 3. The same region of the (k, ω) plane and branch and border lines as in figure 2 for $U/t = 4.9$, $n = 0.59$, and $m \to 0$.

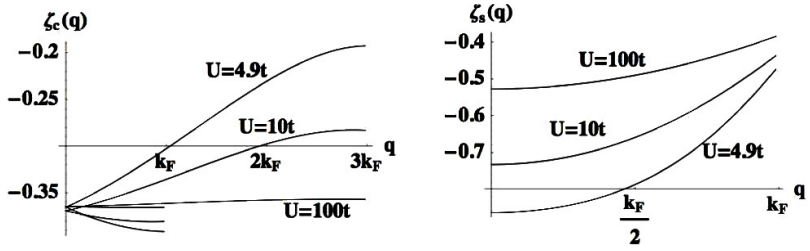

Figure 4. The value of the $c0$ and $s1$ branch line exponents of the one-electron removal weight distribution as a function of momentum for $n = 0.59$, $m \to 0$, and several magnitudes of U/t. The exponents of index c and s refer to the $c0$ and $s1$ branch lines, respectively.

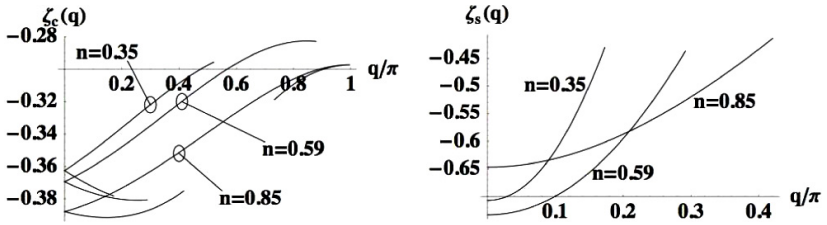

Figure 5. The same exponents as in figure 4 as a function of momentum for $U/t = 10$, $m \to 0$, and several values of n.

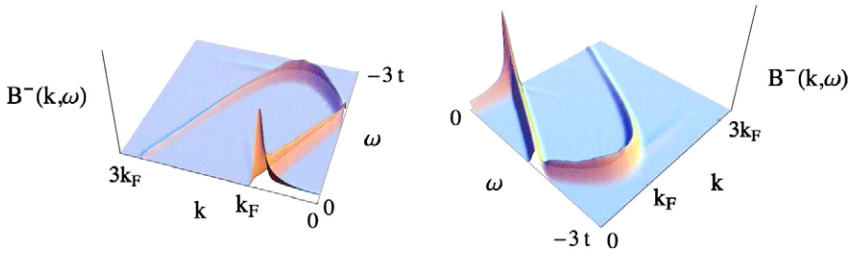

Figure 6. Full PDT one-electron removal spectral-weight distribution associated with the $c0$ and $s1$ momentum deviations of equations (32) and (33) and corresponding functionals given in equations (34) and (35) for $U/t = 100$, $n = 0.59$, and $m \to 0$.

for $U/t \to \infty$. However, the method used in the studies of the latter reference does not apply to finite values of U/t. The one-electron removal spectral-weight distribution related to the TCNQ spectral features is plotted in figure 7 and refers instead to $U/t = 4.9$, $n = 0.59$, and $m \to 0$. It is a part of the full one-electron spectral-weight distribution plotted in figure 1.

Most singular behaviours of the one-electron removal spectral-weight distributions of figures 6 and 7 refer to $c0$ and $s1$ branch lines whose negative power-law exponent magnitude depends on U/t and the momentum. These exponents are plotted in figures 4 and 5. In turn, the weaker lines connecting in figures 2 and 3 the minimum energy points of the two $c0$ lines are border lines. The singularities of the latter lines correspond instead to the U/t and momentum independent exponent $-1/2$, as given in the general border-line expressions (28) and (29) derived in this paper.

Next let us consider the lower-Hubbard-band one-electron addition spectrum for $n = 0.59$; $t = 0.35$ eV; $U/t = 5.61$, from which one derives the TTF related photoemission one-electron removal spectrum for $n = 1.41$; $t = 0.35$ eV; $U/t = 5.61$. Nearly the whole lower-Hubbard-band one-electron addition spectral weight corresponds to the excitations leading to the following deviations from the ground-state $N_{\alpha\nu}\,\alpha\nu$ pseudofermion numbers and $N^{h}_{\alpha\nu}\,\alpha\nu$ pseudofermion-hole

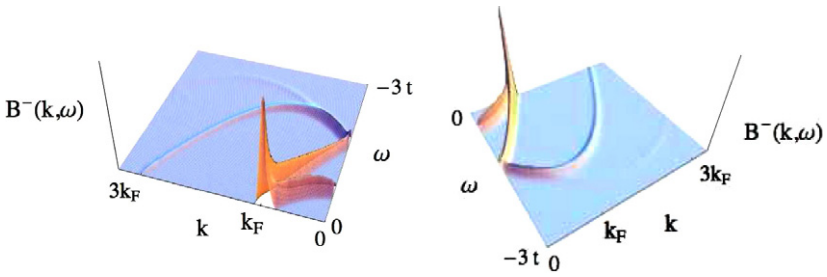

Figure 7. The same PDT one-electron removal spectral-weight distribution as in figure 6 for the values $U/t = 4.9$, $n = 0.59$, and $m \to 0$ suitable for the TCNQ related spectral features.

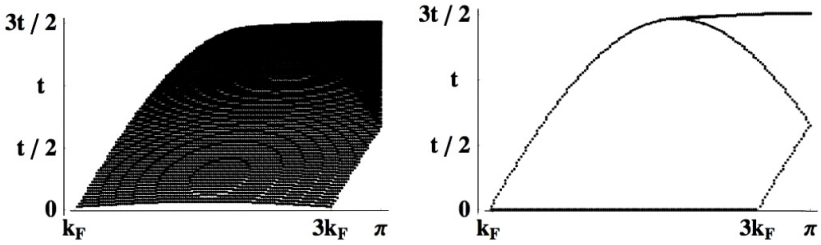

Figure 8. The region of the (k, ω) plane with a finite one-electron addition spectral weight obtained by running over all the momentum values of the $c0$ and $s1$ momentum distribution deviations of equations (32) and (33) for $U/t = 100$, $n = 0.59$, and $m \to 0$. The corresponding branch and border lines are also shown.

numbers where $\alpha\nu = c0, s1$:

$$\Delta N_{c0} = -\Delta N^h_{c0} = +1; \qquad \Delta N_{s1} = 0; \qquad \Delta N^h_{s1} = +1, \tag{36}$$

with the numbers $Q^0_{\alpha\nu}/2$ appearing on the right-hand side of equation (7) reading

$$Q^0_{c0}/2 = 0; \qquad Q^0_{s1}/2 = \pm\pi/2. \tag{37}$$

If we choose the excitation branches that survive for $m \to 0$, the general deviations are for bare-momentum continuum values given by

$$\Delta N_{c0}(q) = \frac{2\pi}{L}\,\delta(q - q_1); \qquad q_1 \in [-2k_{\rm F},\ +\pi]$$
$$\text{and} \qquad q_1 \in [-\pi,\ +2k_{\rm F}]$$
$$\Delta N_{s1}(q) = -\frac{2\pi}{L}\,\delta(q - q'_1) + \frac{\pi}{L}\,\delta(q + k_{\rm F\downarrow}) + \frac{\pi}{L}\,\delta(q - k_{\rm F\downarrow}); \qquad q'_1 \in [-k_{\rm F\downarrow},\ +k_{\rm F\downarrow}], \tag{38}$$

and thus

$$\Delta N_{s1}(q) = -\frac{2\pi}{L}\,\delta(q - q'_1) + \frac{\pi}{L}\,\delta(q - k_{\rm F}) + \frac{\pi}{L}\,\delta(q + k_{\rm F}); \qquad q'_1 \in [-k_{\rm F},\ +k_{\rm F}] \tag{39}$$

as $m \to 0$ for the initial ground state. As for the above one-electron removal case, such deviations and the numbers (37) are used in the general functional $Q_{\alpha\nu}(q_j)/2$ provided in equation (7) and its functional $Q^{\Phi}_{\alpha\nu}(q_j)/2$ defined in equation (4). One then finds

$$Q_{c0}(q)/2 = \pi\Phi_{c0,\,c0}(q, q_1) - \pi\Phi_{c0,\,s1}(q, q'_1) + \pi\Phi_{c0,\,s1}(q, -k_{\rm F\downarrow})/2 + \pi\Phi_{c0,\,s1}(q, +k_{\rm F\downarrow})/2, \tag{40}$$

and

$$Q_{s1}(q)/2 = \pm\pi/2 + \pi\Phi_{s1,\,c0}(q, q_1) - \pi\Phi_{s1,\,s1}(q, q'_1) + \pi\Phi_{s1,\,s1}(q, -k_{\rm F\downarrow})/2 + \pi\Phi_{s1,\,s1}(q, +k_{\rm F\downarrow})/2, \tag{41}$$

respectively.

The creation of the $c0$ pseudofermion and $s1$ pseudofermion-hole refers for $U/t = 100$, $n = 0.59$, and $m \to 0$ to a finite spectral-weight distribution in the region of the (k, ω) plane shown in figure 8. The corresponding lines associated with potential branch lines and border lines are also plotted. In figure 9 the same finite spectral-weight region is shown for the $U/t = 5.61$, $n = 0.59$, and $m \to 0$ values suitable for the TTF related spectral features. The border line connecting the maximum energy point of the $c0$-branch line at momentum $2k_{\rm F}$ with the maximum energy point of the finite spectral-weight distribution at momentum π has in figure 8 $v_{c0}(q) = v_{s1}(q') \approx 0$. Upon decreasing U/t to the value $U/t = 5.61$ suitable for the TTF related spectral features of figure 1, this border line acquires a curvature, as shown in figure 9. Such a curvature and corresponding value of U/t are those behind the agreement achieved in [4] between the PDT predictions and the photoemission spectral features of TTF-TCNQ.

The $c0$ branch lines of the weight distributions of figures 8 and 9 run between the excitation momenta $k_{\rm F}$ and π and between $3k_{\rm F}$ and π, respectively. In turn, the maximum extension of the $s1$ branch line is achieved for large values of U/t when it runs from $k_{\rm F}$ to near $3k_{\rm F}$. The corresponding power-law momentum dependent exponents are plotted in figure 10 for $n = 0.59$, $m \to 0$, and several values of U/t. While the $c0$ branch lines exponents are negative, the $s1$ branch-line exponent is negative for momenta smaller than approximately $k_{\rm F}$ and $2k_{\rm F}$ for $U/t = 5.61$ and $U/t = 100$,

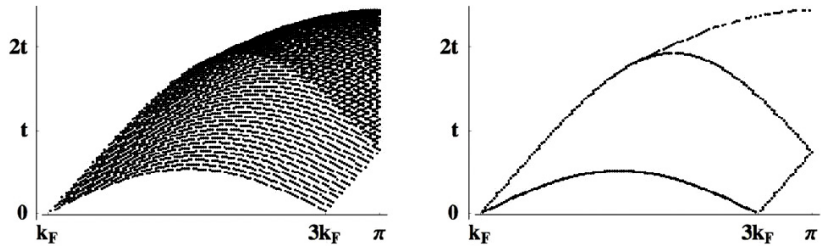

Figure 9. The same region of the (k, ω) plane and branch and border lines as in figure 8 for $U/t = 5.61$, $n = 0.59$, and $m \to 0$.

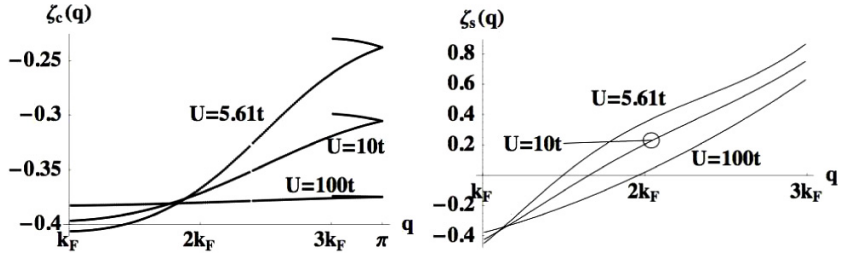

Figure 10. The value of the $c0$ and $s1$ branch line exponents of the one-electron addition spectral-weight distribution as a function of momentum for $n = 0.59$, $m \to 0$, and several magnitudes of U/t. The exponents of index c and s refer to the $c0$ and $s1$ branch lines, respectively.

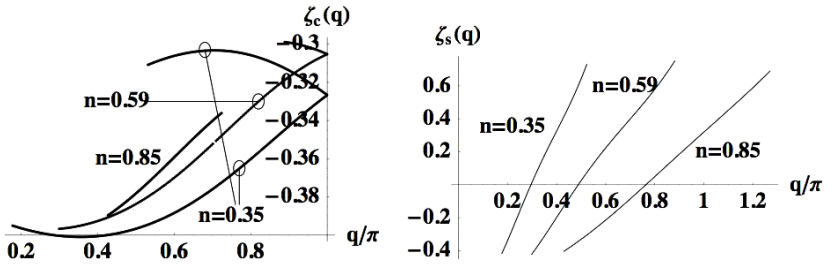

Figure 11. The same exponents as in figure 10 as a function of momentum for $U/t = 10$, $m \to 0$, and several values of n.

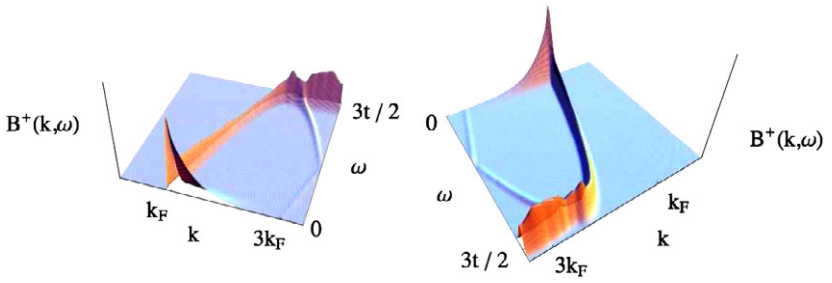

Figure 12. Full PDT one-electron addition spectral-weight distribution associated with the $c0$ and $s1$ momentum deviations of equations (38) and (39) and corresponding functionals given in equations (40) and (41) for $U/t = 100$, $n = 0.59$, and $m \to 0$.

respectively. Again in order to illustrate the evolution of the spectral features upon varying the parameters, the same exponents as in figure 10 are plotted in figure 11 as a function of momentum for $U/t = 10$, $m \to 0$, and several values of n.

The general PDT spectral-function expressions provided in this paper and in [2] lead for $U/t = 100$, $n = 0.59$, and $m \to 0$ and the specific $c0$ and $s1$ momentum deviations of equations (38) and (39) and corresponding functionals provided in equations (40) and (41) to the one-electron addition spectral-weight distribution plotted in figure 12. The large-U/t distribution plotted in that figure is quite similar to the function $A(k, \omega)$ plotted in figure 1 of [16] for $U/t \to \infty$. The one-electron addition spectral-weight distribution related to the TTF spectral features is plotted in figure 13 and refers instead to $U/t = 5.61$, $n = 0.59$, and $m \to 0$. After a straightforward particle–hole transformation, the latter distribution leads to the one-electron removal spectral-weight distribution suitable for the TTF related spectral features. The latter corresponds to $U/t = 5.61$, $n = 1.41$, and $m \to 0$ and is part of the

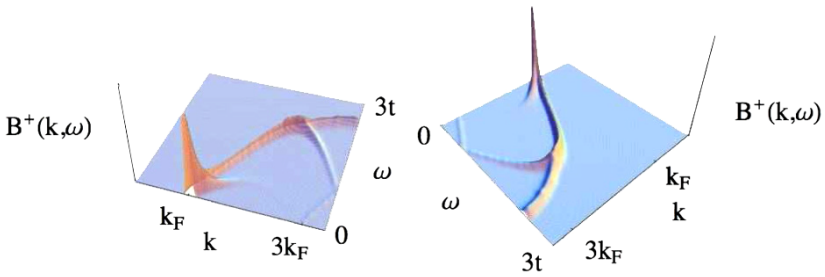

Figure 13. The same PDT one-electron addition spectral-weight distribution as in figure 8 for the values $U/t = 5.61$, $n = 0.59$, and $m \to 0$ suitable for the TTF related spectral features.

full one-electron removal spectral-weight distribution plotted in figure 1.

Most singular behaviours of the one-electron addition spectral-weight distributions of figures 12 and 13 correspond to $c0$ and $s1$ branch lines whose negative power-law exponents are dependent on the U/t and momentum values. These exponents are plotted in figures 10 and 11, and the power-law singularities occur for the momenta where they are negative. In turn, the line connecting in figures 8 and 9 the maximum energy point of the $c0$-branch line at momentum $2k_F$ with the maximum energy point of the finite spectral-weight distribution at momentum π is a border line. The singularities at the latter line correspond to the U/t and momentum independent exponent $-1/2$ and near it the line shape is of the general form provided in expressions (28) and (29).

The four functionals $2\Delta^{\iota}_{\alpha\nu}$ where $\alpha\nu = c0, s1$ and $\iota = \pm 1$ given in equation (10) are in the case of the one-electron excitations behind the spectral-weight distribution plotted in figure 1 fully controlled by the functionals provided in equations (34) and (35) for $U/t = 4.90$, $n = 0.59$, and $m \to 0$ for the TCNQ related spectral features and in equations (40) and (41) for $U/t = 5.61$, $n = 0.59$, and $m \to 0$ for the TTF related spectral features. Since the magnitude of the latter functionals is a function of two momenta q_1 and q'_1 of the deviations of equations (32) and (33) or equations (38) and (39) belonging to the $c0$ and $s1$ band, respectively, it is different for each point of the (k, ω) plane. Moreover, for some of the latter points there are contributions from more than one pair of momenta q_1 and q'_1.

We emphasize that depending on whether none, one, or two of the two above momenta q_1 and q'_1 is or are Fermi points, the corresponding functionals $2\Delta^{\iota}_{\alpha\nu}$ have different forms and the excitation contributes to line shapes described by the expressions provided in equations (66), (70), and (68) of [2], respectively. All such expressions involve the pre-factor function $F_0(z)$ given in equations (A.1)–(A.7) of the appendix. The expressions provided in these equations are a generalization of the pre-factor function $F_0(z)$ provided in equation (62) of [2]. The latter applies when the four functionals $2\Delta^{\iota}_{\alpha\nu}$ where $\alpha\nu = c0, s1$ and $\iota = \pm 1$ are finite. However, in the limit $m \to 0$ that the spectral-weight distributions studied in this paper refer to, one must use in the general expressions provided in equations (66), (70), and (68) of [2] the pre-factor function $F_0(z)$ of equations (A.1)–(A.7) of the appendix.

Note that the above mentioned general expressions provided in equations (68) and (70) of [2] describe the line shape near well defined points and lines in the (k, ω) plane, respectively. When the corresponding exponents are negative, such spectral features refer to the point and branch-line singularities of the weight distributions plotted in figures 1, 6, 7, 12, and 13. In turn, the only type of singularity occurring within the line shape described by the above mentioned general expression provided in equation (66) of [2] is that associated with the border lines studied in the previous section. The corresponding expressions (28) and (29) refer to the vicinity of such border lines.

The complementary studies of [18] provide the specific expressions of the four functionals $2\Delta^{\iota}_{\alpha\nu}$ where $\alpha\nu = c0, s1$ and $\iota = \pm 1$ given in equation (10) for each of the point and branch-line singularities of the TCNQ related one-electron removal spectral features. The functionals given in equations (40) and (41) are the basis of the derivation of similar expressions for the TTF related spectral features. These are straightforwardly derived by choosing particular pairs of momentum values q_1 and q'_1 in the $c0$ and $s1$ momentum deviations of equations (38) and (39), respectively. As discussed above, when such choices involve none, one, or both such momentum pairs being a $c0$ or $s1$ Fermi point, the corresponding four functionals $2\Delta^{\iota}_{\alpha\nu}$ have different forms and the excitation contributes to line shapes described by the expressions provided in equations (66), (70), and (68) of [2] for the two-dimensional weight distribution, vicinity of branch lines, and vicinity of singular points, respectively.

Finally, in figure 14 we plot the theoretical lines corresponding to the sharpest spectral features considered in figure 1 but omit the corresponding detailed spectral-weight distribution over the (k, ω)-plane provided in that figure. The figure also displays the experimental dispersions in the electron removal spectrum of TTF-TCNQ as measured by ARPES in [9]. The border line connecting the maximum energy point of the $c0$-branch line at momentum $2k_F$ with the maximum energy point of the finite spectral-weight distribution at momentum π in figure 9 leads upon the particle–hole transformation to that called the c–s line in figure 14. In turn the border line connecting the minimum energy points of the two $c0$ lines of figure 3 associated with the TCNQ related spectral features is not marked in figure 14, yet the corresponding experimental spectral weight is clearly visible.

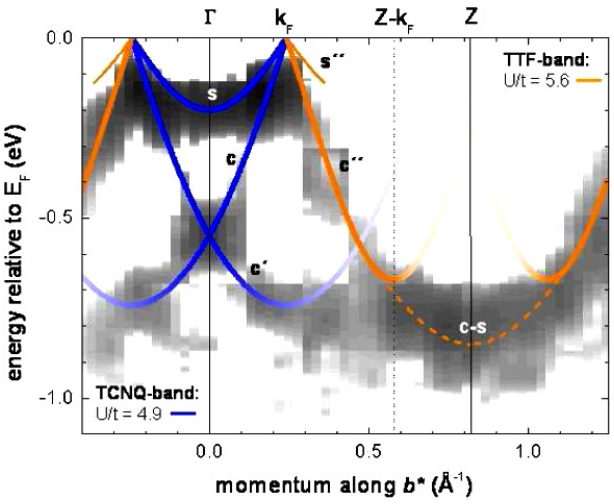

Figure 14. Experimental peak dispersions (grey scale) obtained by ARPES on TTF-TCNQ along the easy-transport axis as given in figure 7 of [9] and matching theoretical branch and border lines. (The Z-point corresponds to the momentum $k = \pi$.) The corresponding detailed theoretical spectral-weight distributions over the whole $(k,\ \omega)$-plane are plotted above in figure 1. While the theoretical charge-c'' and spin-s'' branch lines and c–s border line refer upon the particle–hole transformation to the TTF related spectral features of figures 9 and 13, the charge-c, spin-s, and charge-c' branch lines correspond to the TCNQ related dispersions of figures 3 and 7.

5. Discussion and concluding remarks

In this paper we have generalized the closed-form analytical expressions for the finite-energy one- and two-electron spectral-weight distributions of a 1D correlated metal with on-site electronic repulsion introduced in [2] to all electronic densities of the metallic phase and zero spin density. Moreover, we have studied the particular form of the expressions derived here for the processes contributing to the one-electron spectral-weight distributions related to the TTF and TCNQ stacks of molecules, respectively, in the quasi-1D organic compound TTF-TCNQ investigated in [4]. The corresponding full theoretical one-electron spectral-weight distribution plotted in figure 1 agrees quantitatively for the whole experimental energy bandwidth with the observed one-electron spectral features shown in figure 14.

Other applications of our finite-energy spectral-weight-distribution expressions to several materials, correlated quantum systems, and spectral functions are in progress. This includes the use of our theoretical results in the two-atom spectral-weight distributions measured in 1D optical lattices. Such studies also involve the Hubbard model but with the electrons replaced by fermionic spin-1/2 atoms. While for the one-electron features the branch lines play the major role, in the case of two-electron spectral functions such as the charge dynamical structure factor the two-pseudofermion spectral features of the form given in equation (66) of [2] lead to the main contributions. Generalization of that equation to all electronic densities of the metallic phase and to zero spin density involves the use of the following expression:

$$B^{l}_{\mathcal{N}}(k,\ \omega) \approx \frac{1}{\pi\ C_c\ C_s}\left[\int_{-1/v_{\tilde{\alpha}\tilde{\nu}}}^{+1/v_{\tilde{\alpha}\tilde{\nu}}} \mathrm{d}z\ F_0(z)\right] \times \left(\frac{\Omega}{4\pi\sqrt{v_{c0}\ v_{s1}}}\right)^{\zeta_0(q',\ q'')} \times \frac{\sqrt{v_{c0}\ v_{s1}}}{\zeta_0(q',\ q'')\ |v_{\alpha'\nu'}(q') - v_{\alpha''\nu''}(q'')|}\ ; \qquad l = \pm 1, \tag{42}$$

with the pre-factor function $F_0(z)$ given by the expressions (A.1)–(A.7) of the appendix introduced in this paper. As in equation (28), here q' and q'' stand for the bare-momentum values of the created $\alpha'\nu'$ and $\alpha''\nu''$ pseudofermions or holes, respectively. Indeed, the singular border-line function (28) is a particular case of the general function provided in equation (42), which can be obtained by considering that $v_{\alpha'\nu'}(q') = v_{\alpha''\nu''}(q'')$ in the latter equation.

For finite values of U/t the dominant term of the two-electron spectral functions is often of the general form given in equation (42). However, it can also occur that for intermediate values of U/t such functions are the sum of two or three dominant functions of the general form (42). The main contributions correspond to the two created objects being such that (i) $\alpha'\nu' = c0$ and $\alpha''\nu'' = s1$, (ii) $\alpha'\nu' = \alpha''\nu'' = c0$, and (iii) $\alpha'\nu' = \alpha''\nu'' = s1$. The relative importance of the functions (i)–(iii) and whether the two created objects are pseudofermions and/or pseudofermion holes depends on the specific two-electron spectral function under consideration. Our general expressions (A.1)–(A.7) of the appendix for the pre-factor function $F_0(z)$ appearing on the right-hand side of equation (42) allow the evaluation of all two-electron spectral-weight distributions for initial ground states with zero spin density, which in many situations is the case of physical interest. The branch lines and other spectral features also contribute to the two-electron spectral-weight distributions, yet the dominant contributions are of the general form given in equation (42).

For instance, the preliminary results of [20] consider both one- and two-electron spectral features, profit from the PDT for the one-chain problem, are consistent with the phase diagram observed in the $(TMTTF)_2X$ and $(TMTSF)_2X$ series of organic compounds, and explain the absence of superconductive phases in TTF-TCNQ. The studies of that reference combine the PDT for several one- and two-electron spectral functions with a renormalization group analysis to study the instabilities of a system of weakly coupled Hubbard chains. For low values of the on-site repulsion U and of the doping $\delta = (1 - n)$, the leading instability is towards a superconducting state. The process includes excited states above a small correlation pseudogap. Similar features appear in extended Hubbard models in the vicinity of commensurate fillings. The theoretical predictions of such studies are consistent with the phase diagram observed in the $(TMTTF)_2X$ and $(TMTSF)_2X$ series of organic compounds represented in figure 15. From the results of [20] one can infer that the low-temperature phase of the coupled-chain system will show long-range superconducting order. However, the precise nature of this phase, and the symmetry of the order parameter,

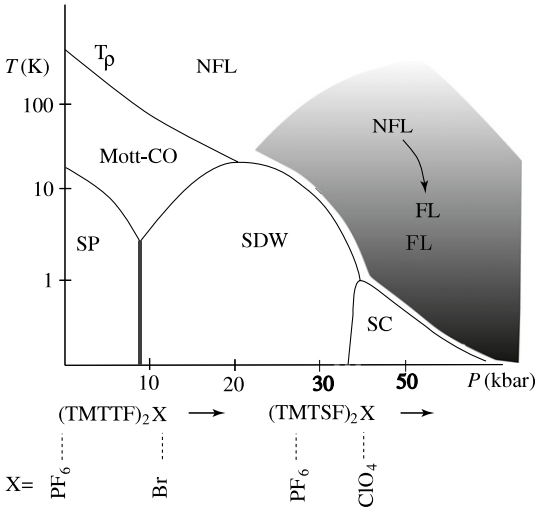

Figure 15. Temperature–pressure phase diagram of the $(TMTTF)_2X$ and $(TMTSF)_2X$ series of compounds. It includes non-Fermi liquid (NPL), insulating Mott–Hubbard (Mott-CO), spin-density-wave (SDW), spin–Peierls, Fermi liquid (FL), and superconducting (SC) phases.

is dependent on the arrangement of the chains within the material. The investigations of [20] use the exponents obtained from the PDT for the one-chain problem and confirm that in 1D non-Fermi liquids weak inter-chain hopping can induce superconductivity. At low temperature these materials show a spin–Peierls or spin-density-wave phase. Under pressure, the $(TMTSF)_2X$ compounds are driven to a superconducting phase, which is removed again if one further increases the pressure.

In addition to the finite-energy spectral features of the organic compound TTF-TCNQ [4] and the preliminary studies of [20] on the $(TMTTF)_2X$ and $(TMTSF)_2X$ series of organic compounds, the general spectral-function expressions derived in this paper will be used elsewhere in the study of specific one- and two-electron spectral functions and its quantitative application to the unusual spectral properties of other low-dimensional materials and systems. While the studies of this paper considered the 1D Hubbard model, which describes successfully some of the exotic properties observed in low-dimensional materials [9, 18–20], our results are of general nature for many integrable interacting problems [1] and therefore have wide applicability.

Acknowledgments

We thank Pedro D Sacramento for stimulating discussions and acknowledge the support of ESF Science Programme INSTANS, European Union Contract 12881 (NEST), FCT grants SFRH/BD/6930/2001, POCTI/FIS/58133/2004, and PTDC/FIS/64926/2006, and OTKA grant T049607.

Appendix. The pre-factor function $F_0(z)$

In this appendix a set of alternative expressions for the pre-factor function $F_0(z)$ on the right-hand side of equation (25) derived by use of equations (19)–(21), (23), and (25) according to the values of the two parameters $2\Delta^{\pm 1}_{\alpha\nu}$ and two parameters $2\Delta^{\pm 1}_{\bar\alpha\bar\nu}$ is given.

(i) When the four parameters $2\Delta^{\pm 1}_{\alpha\nu}$ where $\alpha\nu = c0, s1$ and $\iota = \pm 1$ are finite, we find

$$F_0(z) = 2D_0 \sqrt{\frac{v_{\bar\alpha\bar\nu}}{v_{\alpha\nu}}} \int_0^1 dx \int_{-1}^{+1} dy \times \prod_{\iota'=\pm 1} \frac{\Theta\left(1 - x + \mathrm{sgn}(z)\,\iota'\left[v_{\bar\alpha\bar\nu}|z| - \frac{v_{\bar\alpha\bar\nu}}{v_{\alpha\nu}}\,y\right]\right)}{\Gamma(2\Delta^{\iota'}_{\bar\alpha\bar\nu})} \times \frac{\Theta(x + \mathrm{sgn}(z)\,\iota'\,y)}{\Gamma(2\Delta^{\iota'}_{\alpha\nu})} \left(\sqrt{\frac{v_{\alpha\nu}}{v_{\bar\alpha\bar\nu}}}\left[1 - x + \mathrm{sgn}(z)\,\iota' \times \left[v_{\bar\alpha\bar\nu}|z| - \frac{v_{\bar\alpha\bar\nu}}{v_{\alpha\nu}}\,y\right]\right]\right)^{2\Delta^{\iota}_{\bar\alpha\bar\nu}-1} \times \left(\sqrt{\frac{v_{\bar\alpha\bar\nu}}{v_{\alpha\nu}}}\left[x + \mathrm{sgn}(z)\,\iota'\,y\right]\right)^{2\Delta^{\iota'}_{\alpha\nu}-1}. \quad (A.1)$$

(ii) When $2\Delta^{-\bar\iota}_{\bar\alpha\bar\nu} = 0$ and the remaining three parameters are finite,

$$F_0(z) = 2D_0 \frac{v_{\bar\alpha\bar\nu}}{v_{\alpha\nu}} \int_{-1}^{+1} dy \times \left\{\Theta\left(\bar\iota\left[\mathrm{sgn}(z)y - v_{\alpha\nu}\left(z - \frac{\bar\iota}{v_{\bar\alpha\bar\nu}}\right)\right]\right) \times \Theta(\bar\iota\,[z v_{\alpha\nu} - \mathrm{sgn}(z)y])\right\} \left\{\Gamma(2\Delta^{\bar\iota}_{\bar\alpha\bar\nu})\right\}^{-1} \times \left(\sqrt{\frac{v_{\alpha\nu}}{v_{\bar\alpha\bar\nu}}}\,2\bar\iota\left[z - \mathrm{sgn}(z)\frac{y}{v_{\alpha\nu}}\right]v_{\bar\alpha\bar\nu}\right)^{2\Delta^{\bar\iota}_{\bar\alpha\bar\nu}-1} \times \prod_{\iota'=\pm 1} \frac{\Theta\left(1 + \mathrm{sgn}(z)\left[\iota' + \bar\iota\,\frac{v_{\bar\alpha\bar\nu}}{v_{\alpha\nu}}\right]y - \bar\iota\,v_{\bar\alpha\bar\nu}\,z\right)}{\Gamma(2\Delta^{\iota'}_{\alpha\nu})} \times \left(\sqrt{\frac{v_{\bar\alpha\bar\nu}}{v_{\alpha\nu}}}\left[1 + \mathrm{sgn}(z)\left[\iota' + \bar\iota\,\frac{v_{\bar\alpha\bar\nu}}{v_{\alpha\nu}}\right]y - \bar\iota\,v_{\bar\alpha\bar\nu}\,z\right]\right)^{2\Delta^{\iota'}_{\alpha\nu}-1}. \quad (A.2)$$

(iii) When $2\Delta^{-\iota}_{\alpha\nu} = 0$ and the remaining three parameters are finite,

$$F_0(z) = 2D_0 \int_{-1}^{+1} dy \frac{\Theta\left(\iota\,\mathrm{sgn}(z)y\right)}{\Gamma(2\Delta^{\iota}_{\alpha\nu})} \times \left(\sqrt{\frac{v_{\bar\alpha\bar\nu}}{v_{\alpha\nu}}}\,\iota\,\mathrm{sgn}(z)2y\right)^{2\Delta^{\iota}_{\alpha\nu}-1} \times \prod_{\bar\iota'=\pm 1} \frac{\Theta\left(1 - \mathrm{sgn}(z)\left[\iota + \bar\iota'\,\frac{v_{\bar\alpha\bar\nu}}{v_{\alpha\nu}}\right]y + \bar\iota'\,v_{\bar\alpha\bar\nu}\,z\right)}{\Gamma(2\Delta^{\bar\iota'}_{\bar\alpha\bar\nu})} \times \left(\sqrt{\frac{v_{\alpha\nu}}{v_{\bar\alpha\bar\nu}}}\left[1 - \mathrm{sgn}(z)\left[\iota + \bar\iota'\,\frac{v_{\bar\alpha\bar\nu}}{v_{\alpha\nu}}\right]y + \bar\iota'\,v_{\bar\alpha\bar\nu}\,z\right]\right)^{2\Delta^{\bar\iota'}_{\bar\alpha\bar\nu}-1}. \quad (A.3)$$

(iv) When both $2\Delta^{\pm 1}_{\bar{\alpha}\bar{\nu}} = 0$ and the remaining two parameters are finite,

$$F_0(z) = D_0 \sqrt{\frac{v_{\bar{\alpha}\bar{\nu}}}{v_{\alpha\nu}}}\Theta\Big(\frac{1}{v_{\alpha\nu}} - |z|\Big) \times \prod_{\iota'=\pm 1} \frac{1}{\Gamma(2\Delta^{\iota'}_{\alpha\nu})}\left(\sqrt{\frac{v_{\bar{\alpha}\bar{\nu}}}{v_{\alpha\nu}}}\Big[1 + \iota' v_{\alpha\nu}\, z\Big]\right)^{2\Delta^{\iota'}_{\alpha\nu}-1}. \tag{A.4}$$

(v) When both $2\Delta^{\pm 1}_{\alpha\nu} = 0$ and the remaining two parameters are finite,

$$F_0(z) = D_0 \sqrt{\frac{v_{\alpha\nu}}{v_{\bar{\alpha}\bar{\nu}}}} \prod_{\bar{\iota}'=\pm 1} \frac{\Theta\Big(\frac{1}{v_{\bar{\alpha}\bar{\nu}}} - \bar{\iota}' z\Big)}{\Gamma(2\Delta^{\bar{\iota}'}_{\bar{\alpha}\bar{\nu}})} \times \left(\sqrt{\frac{v_{\alpha\nu}}{v_{\bar{\alpha}\bar{\nu}}}}\Big[1 - \bar{\iota}' v_{\bar{\alpha}\bar{\nu}}\, z\Big]\right)^{2\Delta^{\bar{\iota}'}_{\bar{\alpha}\bar{\nu}}-1} = 0. \tag{A.5}$$

(vi) When $2\Delta^{-\iota}_{\alpha\nu} = 2\Delta^{-\bar{\iota}}_{\bar{\alpha}\bar{\nu}} = 0$ and the remaining two parameters are finite,

$$F_0(z) = \frac{2D_0}{\sqrt{v_{\alpha\nu} v_{\bar{\alpha}\bar{\nu}}}}\left(\frac{v_{\alpha\nu} - \iota\bar{\iota}\, v_{\bar{\alpha}\bar{\nu}}}{v_{\alpha\nu} v_{\bar{\alpha}\bar{\nu}}}\right)^{1-\zeta_0} \times \frac{\Theta\Big(\bar{\iota}[z - \frac{\iota}{v_{\alpha\nu}}]\Big)}{\Gamma(2\Delta^{\bar{\iota}}_{\bar{\alpha}\bar{\nu}})}\frac{\Theta\Big(\frac{1}{v_{\bar{\alpha}\bar{\nu}}} - \bar{\iota} z\Big)}{\Gamma(2\Delta^{\iota}_{\alpha\nu})} \times \left(2\sqrt{\frac{v_{\alpha\nu}}{v_{\bar{\alpha}\bar{\nu}}}}\,\bar{\iota}\left[z - \frac{\iota}{v_{\alpha\nu}}\right]\right)^{2\Delta^{\bar{\iota}}_{\bar{\alpha}\bar{\nu}}-1} \times \left(2\sqrt{\frac{v_{\bar{\alpha}\bar{\nu}}}{v_{\alpha\nu}}}\left[\frac{1}{v_{\bar{\alpha}\bar{\nu}}} - \bar{\iota} z\right]\right)^{2\Delta^{\iota}_{\alpha\nu}-1}. \tag{A.6}$$

(vii) When both $2\Delta^{\iota}_{\alpha\nu} > 0$ (and $2\Delta^{\bar{\iota}}_{\bar{\alpha}\bar{\nu}} > 0$) and the remaining three parameters vanish,

$$F_0(z) = \frac{D_0}{v_{\alpha\nu}\Gamma(2\Delta^{\iota}_{\alpha\nu})}\left(2\sqrt{\frac{v_{\bar{\alpha}\bar{\nu}}}{v_{\alpha\nu}}}\right)^{2\Delta^{\iota}_{\alpha\nu}-1}\delta\left(z - \frac{\iota}{v_{\alpha\nu}}\right), \tag{A.7}$$

(and a similar expression with $\alpha\nu$, ι, and $\bar{\alpha}\bar{\nu}$ replaced by $\bar{\alpha}\bar{\nu}$, $\bar{\iota}$, and $\alpha\nu$, respectively).

References

[1] Voit J 1995 *Rep. Prog. Phys.* **58** 977 and references therein

[2] Carmelo J M P, Penc K and Bozi D 2005 *Nucl. Phys.* B **725** 421
Carmelo J M P, Penc K and Bozi D 2006 *Nucl. Phys.* B **737** 351 (erratum)

[3] Carmelo J M P and Penc K 2006 *Eur. Phys. J.* B **51** 477

[4] Bozi D, Carmelo J M P, Penc K and Sacramento P D 2008 *J. Phys.: Condens. Matter* **20** 022205

[5] Pereira R G, Sirker J, Caux J S, Hagemans R, Maillet J M, White S R and Affleck I 2006 *Phys. Rev. Lett.* **96** 257202
Pereira R G, White S R and Affleck I 2008 *Phys. Rev. Lett.* **100** 027206
White S R and Affleck I 2008 *Phys. Rev.* B **77** 134437

[6] Pustilnik M, Khodas M, Kamenev A and Glazman L I 2006 *Phys. Rev. Lett.* **96** 196405
Khodas M, Pustilnik M, Kamenev A and Glazman L I 2007 *Phys. Rev. Lett.* **99** 110405
Khodas M, Pustilnik M, Kamenev A and Glazman L I 2007 *Phys. Rev.* B **76** 155402
Imambekov A and Glazman L I 2008 *Phys. Rev. Lett.* **100** 206805

[7] Carmelo J M P, Martelo L M and Penc K 2006 *Nucl. Phys.* B **737** 237
Carmelo J M P and Penc K 2006 *Phys. Rev.* B **73** 113112

[8] Zwick F, Jérome D, Margaritondo G, Onellion M, Voit J and Grioni M 1998 *Phys. Rev. Lett.* **81** 2974
Claessen R, Sing M, Schwingenschlögl U, Blaha P, Dressel M and Jacobsen C S 2002 *Phys. Rev. Lett.* **88** 096402

[9] Sing M, Schwingenschlögl U, Claessen R, Blaha P, Carmelo J M P, Martelo L M, Sacramento P D, Dressel M and Jacobsen C S 2003 *Phys. Rev.* B **68** 125111

[10] Jaksch D and Zoller P 2005 *Ann. Phys.* **315** 52
Liu X-J, Drummond Peter D and Hu H 2005 *Phys. Rev. Lett.* **94** 136406

[11] Lieb Elliot H and Wu F Y 1968 *Phys. Rev. Lett.* **20** 1445
Martins M J and Ramos P B 1998 *Nucl. Phys.* B **522** 413

[12] Takahashi M 1972 *Prog. Theor. Phys.* **47** 69

[13] Heilmann O J and Lieb E H 1971 *Ann. New York Acad. Sci.* **172** 583
Yang C N 1989 *Phys. Rev. Lett.* **63** 2144

[14] Carmelo J M P, Román J M and Penc K 2004 *Nucl. Phys.* B **683** 387

[15] Carmelo J M P and Sacramento P D 2003 *Phys. Rev.* B **68** 085104

[16] Penc K, Hallberg K, Mila F and Shiba H 1996 *Phys. Rev. Lett.* **77** 1390

[17] Penc K, Hallberg K, Mila F and Shiba H 1997 *Phys. Rev.* B **55** 15 475

[18] Carmelo J M P, Penc K, Sacramento P D, Sing M and Claessen R 2006 *J. Phys.: Condens. Matter* **18** 5191

[19] Benthien H, Gebhard F and Jeckelmann E 2004 *Phys. Rev. Lett.* **92** 256401

[20] Carmelo J M P, Guinea F, Penc K and Sacramento P D 2004 *Europhys. Lett.* **68** 839

[21] Belavin A A, Polyakov A M and Zamolodchikov A B 1984 *Nucl. Phys.* B **241** 333

[22] Schulz H J 1990 *Phys. Rev. Lett.* **64** 2831
Carmelo J M P, Castro Neto A H and Campbell D K 1994 *Phys. Rev. Lett.* **73** 926
Carmelo J M P, Castro Neto A H and Campbell D K 1994 *Phys. Rev.* B **50** 3683

[23] Carmelo J M P 2005 *J. Phys.: Condens. Matter* **17** 5517

[24] Jordan P and Wigner E 1928 *Z. Phys.* **47** 631